INTERNATIONAL JOURNAL FOR NUMERICAL AND ANALYTICAL METHODS IN GEOMECHANICS
Int. J. Numer. Anal. Meth. Geomech. 2010; **34**:1009–1040
Published online 9 October 2009 in Wiley InterScience (www.interscience.wiley.com). DOI: 10.1002/nag.841

A destructuration theory and its application to SANICLAY model

Mahdi Taiebat[1,*,†], Yannis F. Dafalias[2,3] and Ralf Peek[4]

[1]*Department of Civil Engineering, University of British Columbia, Vancouver, B.C., Canada V6T 1Z4*
[2]*Department of Civil and Environmental Engineering, University of California, Davis, CA 95616, U.S.A.*
[3]*Department of Mechanics, National Technical University of Athens, Zographou 15780, Hellas*
[4]*Shell International Exploration and Production, B.V., The Netherlands*

SUMMARY

Many natural clays have an undisturbed shear strength in excess of the remoulded strength. Destructuration modeling provides a means to account for such sensitivity in a constitutive model. This paper extends the SANICLAY model to include destructuration. Two distinct types of destructuration are considered: isotropic and frictional. The former is a concept already presented in relation to other models and in essence constitutes a mechanism of isotropic softening of the yield surface with destructuration. The latter refers to the reduction of the critical stress ratio reflecting the effect of destructuration on the friction angle, and is believed to be a novel proposition. Both the types depend on a measure of destructuration rate expressed in terms of combined plastic volumetric and deviatoric strain rates. The SANICLAY model itself is generalized from its previous form by additional dependence of the yield surface on the third isotropic stress invariant. Such a generalization allows to obtain as particular cases simplified model versions of lower complexity including one with a single surface and associative flow rule, by simply setting accordingly parameters of the generalized version. A detailed calibration procedure of the relatively few model constants is presented, and the performance of three versions of the model, in descending order of complexity, is validated by comparison of simulations to various data for oedometric consolidation followed by triaxial undrained compression and extension tests on two structured clays. Copyright © 2009 John Wiley & Sons, Ltd.

Received 27 November 2008; Revised 14 April 2009; Accepted 10 August 2009

KEY WORDS: clays; constitutive relations; plasticity; destructuration; anisotropy

*Correspondence to: Mahdi Taiebat, Department of Civil Engineering, University of British Columbia, Vancouver, B.C., Canada V6T 1Z4.
†E-mail: mtaiebat@civil.ubc.ca

Contract/grant sponsor: Shell Exploration and Production Company (USA)
Contract/grant sponsor: NSF; contract/grant number: CMS-0201231

1. INTRODUCTION

Advanced geotechnical design on soft clays has often been based on using isotropic and unstructured elastoplastic soil models, such as the modified cam clay (MCC) model (Burland [1]). Natural soft clays, however, almost always have a significant degree of anisotropy and in several cases a natural structure formed during deposition and subsequent one-dimensional (oedometric) consolidation, and the development of chemical bonds between particles due to various reasons. While bonding due to cementation can be responsible for sensitivity in some cases, the physico-chemical effects can be the cause in other cases. For example, a flocculated structure forms in the marine environment. When the salt is leached away, an imbalance in physico-chemical forces ensues, leading to sensitivity. Neglecting the effect of anisotropy, structure and their evolution from soil behavior may lead to incorrect predictions of soil response under loading (see, e.g. Zdravkovic *et al.* [2] and Leroueil *et al.* [3]).

Anisotropy can be accounted for by rotational hardening, which implies a rotation of the yield and plastic potential surfaces. Rotationally hardening models for clays appear to have been first proposed by Sekiguchi and Ohta [4], who are also referenced by Hashiguchi [5]. However, the number of applications since then is too numerous to be listed here. Dafalias [6] proposed what can be thought to be the simplest possible energetic extension of the Modified Cam Clay (MMC) model from isotropic to anisotropic response, introducing in the rate of plastic work expression a contribution coupling the volumetric and deviatoric plastic strain rates. The resulting plastic potential surface in the triaxial $p-q$ space, which for associative plasticity serves also as a yield surface, is a rotated and distorted ellipse. The amount of rotation and distortion portrays the extent of anisotropy, and is controlled by an evolving variable α, which is scalar-valued in triaxial and tensor-valued in multiaxial stress space. Employing the plastic potential surface proposed by Dafalias [6], a number of models were developed subsequently by Dafalias [7], Korhonen and Lojander [8], Thevanayagam and Chameau [9], Newson and Davies [10], Wheeler *et al.* [11], and Wheeler *et al.* [12]. These models differed mainly in the rotational hardening law for α, and adopted the associative flow rule except from the work of Newson and Davies [10], who introduced a yield surface based on the experimental observations. More recently Dafalias *et al.* [13–15] proposed the SANICLAY model based on their earlier works in which a non-associated flow rule allows the simulation of softening response under undrained compression following oedometric consolidation.

Much of the emphasis in constitutive modeling has been on reconstituted soils, rather than soils in their natural state. This has the advantage that it is much easier to repeatably produce samples, and thus the models can more readily be tested for different loading paths. However, in engineering applications one typically encounters natural soils, which often behave quite differently. Natural structure of *in-situ* soils, which is the main focus of this study, renders their behavior different from that of the reconstituted material. A key difference is that many natural clays have an undisturbed shear strength in excess of the remoulded strength. Terzaghi [16] has defined the sensitivity of clay as the ratio of their undisturbed and remoulded strength. The sensitivity varies from about 1 for heavily over-consolidated clays to values of over 100 for the so-called extra-sensitive or *quick* clays [17]. In fact most clays, except those which have been heavily over-consolidated, lose a proportion of their strength when remoulded. Clays that have been heavily over-consolidated during their geological history, such as London Clay, are insensitive (sensitivity = 1). There seem to be few examples of clays of low sensitivity (sensitivity = 1–2), but sensitivities of 2–4 are very common among normally consolidated clays, and sensitivities of 4 to 8 are quite frequently

DOI: 10.1002/nag

encountered. Extra-sensitive clays (sensitivity>8) are met very commonly in parts of Scandinavia and Canada [17]. Burland [18] attributed the *structure* of natural soils to two constituents: 1. the *fabric*, consisting of the spatial arrangement of soil particles and inter-particle contacts, which is the underlying reason for macroscopic anisotropy; 2. the *bonding* between particles, which can be progressively destroyed during plastic straining. The term *destructuration* is now often limited to the progressive damage to bonding during plastic straining [19], and this is the sense in which it is used here.

Such a loss of strength due to the destructuration process may be critical for design. Destructuration manifests itself as a sudden post-yield increase in compressibility, or a post-peak decrease in strength under shearing. This is particularly true in soft clays such as Leda clay (Mitchell [20]), Bothkennar clay [21], and Pisa clay [22]. Some stiff clays have also been considered *structured* in the literature (e.g. Pietrafitta clay [23]; Vallericca clay [23, 24]; Pappadai clay [25]). The presence of bonding allows the natural soil to exist at a higher void ratio than would otherwise be possible [18, 26], and damage of this bonding during plastic straining leads to additional compression as some of the bonding effect is lost. Damage to the bonding can be caused by both plastic volumetric and plastic shear strains, both of which involve slippage at inter-particle contacts and consequent breakage of bonds. A typical example of the effects induced by initial structure is the extreme sensitivity of Scandinavian quick clays [27]. Some aspects of the response of structured clays are presented in Figure 1. In particular, Figure 1(a) presents the results of K_0 consolidation tests on structured (intact) and reconstituted samples of Bothkennar clay in $e-p$ space. Figure 1(b) shows the associated softening in the $p-q$ space for undrained triaxial compression and extension tests on Bothkennar clay [21].

A common way of introducing destructuration of initial structure into the elastoplastic constitutive modeling is to assume that the size of the yield surface depends on the amount of damage

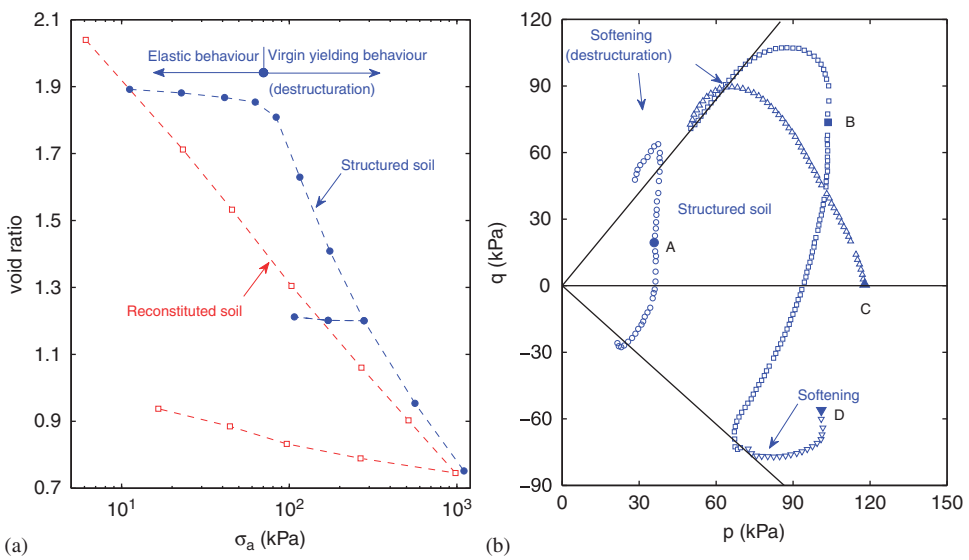

Figure 1. Behavior of structured (intact) and reconstituted samples Bothkennar clay: (a) Oedometer tests, (b) undrained triaxial compression and extension tests (data after [21]).

DOI: 10.1002/nag

(for instance through a progressive decay of a cohesive component of strength [28], or that both the size and the location of the yield locus depend on the amount of damage [29]. Along these lines there have been important developments in formulating appropriate constitutive models (e.g. Nova [30], Gens and Nova [29], Lagioia and Nova [31], Rouainia and Muir Wood [32], Kavvadas and Amorosi [33], Cotecchia and Chandler [25], Gajo and Wood [34], Amorosi and Kavvadas [35], Callisto *et al.* [36], Liu and Carter [37], Callisto and Rampello [38], and Baudet and Stallbrass [39]). The various models differ in the precise form of destructuration law applied and in the form of the underlying reference model used for the un-bonded (intrinsic) material. Anisotropy is not a part of several models while for some others is due to structure and as soon as destructuration is complete, anisotropy disappears. This does not fit with the experimental observations on soft clays, which show that the anisotropy of reconstituted samples subjected to an anisotropic stress history can be as great as the anisotropy of corresponding natural (bonded) samples [19].

In most works, the modeling of destructuration is in essence an isotropic softening mechanism by which the size of the yield surface decreases as a result of destructuration, the rate of which is expressed by means of a combined volumetric and deviatoric plastic strain rate measure. Such an isotropic softening co-exists with isotropic hardening due to consolidation in a two-way competing process. This aspect of isotropic destructuration will be adopted in the present work. It will then be supplemented by what it appears to be a novel constitutive ingredient, called frictional destructuration, which addresses the reduction of the critical state stress ratio as a reflection of reduction of friction angle due to destructuration. The constitutive formulation of the isotropic and frictional destructuration is presented in Section 2 in a generic way that can be associated with a general class of constitutive models in both triaxial and multiaxial space. Subsequently, the proposed destructuration mechanism is introduced specifically in a generalized form of the SANICLAY model which, compared with the earlier version [6], includes the dependence of the yield surface on the third stress invariant and is presented in Section 3. An advantage of such a generalization is that it allows the user to obtain several simplified versions of the general model by appropriately choosing various parameters of the formulation. This is shown in Section 3.4, where two special cases of the model formulation can be thus obtained, including one with a single surface and associated flow rule. A step-by-step calibration process for the model constants is presented in Section 4. The performance of the proposed formulation is validated against the results of a number of laboratory experiments on remoulded and intact samples of Bothkennar clay.

Although destructuration can lead to softening, and softening can lead to localization of deformations (associated with loss of ellipticity of the governing equations for the incremental deformations in a boundary value problem), localization is not specifically addressed in the present study. No localization of deformations has been reported in the tests for which the calibrations are performed.

2. GENERIC FORMULATION OF DESTRUCTURATION MECHANISM

In this section, an appropriate mechanism for capturing the destructuration is proposed. This mechanism is defined in a generic sense for a general class of soil constitutive models and is presented first in triaxial stress/strain space and then is generalized to the multiaxial space. In the sequel $\boldsymbol{\sigma}$ and $\boldsymbol{\varepsilon}$ are generic symbols for the stress and strain tensors and their components thereof, while a superposed dot denotes the material time derivative, or rate. Note that in this paper all

DOI: 10.1002/nag

stress components are considered effective and as usual in geomechanics, both stress and strain quantities are assumed positive in compression.

2.1. Formulation in the triaxial space

It is very common in geomechanics to formulate the constitutive relations first in the triaxial space in terms of the following stress and strain quantities:

$$p = \tfrac{1}{3}(\sigma_1 + 2\sigma_3), \quad q = (\sigma_1 - \sigma_3) \tag{1}$$

$$\varepsilon_v = (\varepsilon_1 + 2\varepsilon_3), \quad \varepsilon_q = \tfrac{2}{3}(\varepsilon_1 - \varepsilon_3) \tag{2}$$

where recall that $\sigma_2 = \sigma_3$ and $\varepsilon_2 = \varepsilon_3$. Here, (p, q) and $(\varepsilon_v, \varepsilon_q)$ are energy-conjugate, in the sense that $\boldsymbol{\sigma} : \boldsymbol{\varepsilon}$ represents the increment on work per unit volume done on the material.

2.1.1. Unstructured reference model. With the total strain rate additive decomposition $\dot{\boldsymbol{\varepsilon}} = \dot{\boldsymbol{\varepsilon}}^e + \dot{\boldsymbol{\varepsilon}}^p$ into elastic (superscript e) and plastic (superscript p) parts, the isotropic hypoelastic relations

$$\dot{\varepsilon}_v^e = \frac{\dot{p}}{K}, \quad \dot{\varepsilon}_q^e = \frac{\dot{q}}{3G} \tag{3}$$

are adopted, with K and G the hypoelastic bulk and shear moduli, respectively.

The volumetric and deviatoric plastic strain rates are given by the flow rule

$$\dot{\varepsilon}_v^p = \langle L \rangle \frac{\partial g}{\partial p}, \quad \dot{\varepsilon}_q^p = \langle L \rangle \frac{\partial g}{\partial q} \tag{4}$$

where g is the plastic potential, and L is the plastic loading index (or plastic multiplier), enclosed in the Maccauley brackets $\langle\rangle$ to be defined in the following. The plastic potential surface is analytically given by a relation

$$g(p, q, \alpha, p_\alpha, M) = 0 \tag{5}$$

where M is the critical stress ratio, α is a stress-ratio type internal variable (it will be a tensor-valued quantity in the multiaxial stress space), which accounts for evolving anisotropy by controlling the rotational hardening of the plastic potential and is assumed to be bounded by M, and p_α is chosen such that $g = 0$ passes through the current stress point. The yield surface equation, which in general is different from the plastic potential for non-associative flow rule, is given by an equation of the form

$$f(p, q, \beta, p_0, N) = 0 \tag{6}$$

where p_0 and the stress-ratio type of internal variable β, which will be a tensor-valued quantity in the multiaxial stress space, represent the isotropic and rotational hardening variables, respectively, while N is a constant similar in nature to M, and serves as the bound for β. The rate equations for the internal variables are as follows:

$$\dot{p}_0 = \langle L \rangle \bar{p}_0 \tag{7a}$$

$$\dot{\alpha} = \langle L \rangle \bar{\alpha} \tag{7b}$$

$$\dot{\beta} = \langle L \rangle \bar{\beta} \tag{7c}$$

DOI: 10.1002/nag

where $\bar{p}_0$, $\bar{\alpha}$, and $\bar{\beta}$ are to be defined according to the model used. Finally, the determination of the loading index L is obtained by considering the consistency condition $\dot{f}=0$ in which Equations (7a) and (7c) are substituted to yield

$$L=\frac{1}{K_p}\left(\frac{\partial f}{\partial p}\dot{p}+\frac{\partial f}{\partial q}\dot{q}\right) \tag{8a}$$

$$K_p=-\left(\frac{\partial f}{\partial p_0}\bar{p}_0+\frac{\partial f}{\partial \beta}\bar{\beta}\right) \tag{8b}$$

with K_p the plastic modulus. Notice that the evolution of α does not effect the value of K_p directly.

2.1.2. General approach to introduce structuration. The effect of structure will be expressed by changing the value of p_0 to p_0^* by means of an isotropic structuration factor S_i, and the values of M and N to M^* and N^*, respectively, by means of a frictional structuration factor S_f according to the relations

$$p_0^*=S_i\,p_0 \tag{9a}$$

$$N^*=S_f N \tag{9b}$$

$$M^*=S_f M \tag{9c}$$

where $S_i\geqslant 1$ and $S_f\geqslant 1$. Often the S_i and S_f are referred to as structuration factors. Equation (9a) has been proposed in previous works while Equations (9b) and (9c) appear to be novel. A value of unity for either S_i or S_f implies the unstructured soil state. The structuration factors will be considered as internal variables evolving according to the equations

$$\dot{S}_i=\langle L\rangle\bar{S}_i \tag{10a}$$

$$\dot{S}_f=\langle L\rangle\bar{S}_f \tag{10b}$$

with $\bar{S}_i$ and $\bar{S}_f$ to be defined in the sequel. Whatever their definition may be, since destructuration diminishes the values of S_i and S_f toward unity, it follows that the $\bar{S}_i$ and $\bar{S}_f$ must be negative. By taking the rate of Equations (9a)–(9c) and using Equation (10a) one has

$$\dot{p}_0^*=\dot{S}_i\,p_0+S_i\,\dot{p}_0=\langle L\rangle(\bar{S}_i\,p_0+S_i\,\bar{p}_0)=\langle L\rangle\,\bar{p}_0^* \tag{11a}$$

$$\dot{N}^*=\dot{S}_f N=\langle L\rangle\bar{S}_f N=\langle L\rangle\bar{N}^* \tag{11b}$$

$$\dot{M}^*=\dot{S}_f M=\langle L\rangle\bar{S}_f M=\langle L\rangle\bar{M}^* \tag{11c}$$

where

$$\bar{p}_0^*=\bar{S}_i\,p_0+S_i\,\bar{p}_0 \tag{12a}$$

$$\bar{N}^*=\bar{S}_f N \tag{12b}$$

$$\bar{M}^*=\bar{S}_f M \tag{12c}$$

DOI: 10.1002/nag

Equations (11a) and (12a) clearly show the effect of isotropic destructuration on isotropic hardening expressed by the evolution of p_0^*. Recalling that the $\bar{S}_i \leqslant 0$ while S_i, p_0, and $\bar{p}_0$ are positive (for the $\bar{p}_0$ this is true under consolidation), Equation (11a) portrays the competition between the process of destructuration that tends to decrease p_0^* via the first term $\bar{S}_i p_0$, and consolidation that tends to increase p_0^* via the second term $S_i \bar{p}_0$. The frictional destructuration has no bearing on such an isotropic hardening but it does have an effect on the anisotropic evolution expressed by Equations (7b) and (7c). Recalling that the M and N are bounds on the evolving values of α and β for the unstructured clay, it is then expected that for the structured one it is the M^* and N^* which will serve as corresponding bounds. As frictional destructuration diminishes the values of M^* and N^* while the evolution Equations (7b) and (7c) are not affected by it, it is conceivable that such an unrelated evolution of these quantities may lead to having α and β reaching values greater than M^* and N^*, respectively. To prevent that from happening, one can introduce additional terms in the evolution Equations (7b) and (7c) for α and β such that proportionality of change due to destructuration for M^*, N^*, α, and β is postulated, which can be expressed analytically by

$$\frac{\dot{M}^*}{M^*} = \frac{\dot{N}^*}{N^*} = \frac{\dot{\alpha}_f}{\alpha} = \frac{\dot{\beta}_f}{\beta} \tag{13}$$

where $\dot{\alpha}_f$ and $\dot{\beta}_f$ are the aforementioned additional terms for $\dot{\alpha}$ and $\dot{\beta}$. The foregoing Equations (13) in conjunction with Equations (11b) and (11c) yields:

$$\dot{\alpha}_f = \alpha \frac{\dot{M}^*}{M^*} = \alpha \frac{\dot{S}_f M}{S_f M} = \frac{\dot{S}_f}{S_f}\alpha = \langle L \rangle \frac{\bar{S}_f}{S_f}\alpha = \langle L \rangle \bar{\alpha}_f \Rightarrow \bar{\alpha}_f = \frac{\bar{S}_f}{S_f}\alpha \tag{14a}$$

$$\dot{\beta}_f = \beta \frac{\dot{N}^*}{N^*} = \beta \frac{\dot{S}_f N}{S_f N} = \frac{\dot{S}_f}{S_f}\beta = \langle L \rangle \frac{\bar{S}_f}{S_f}\beta = \langle L \rangle \bar{\beta}_f \Rightarrow \bar{\beta}_f = \frac{\bar{S}_f}{S_f}\beta \tag{14b}$$

Hence, a combination of Equations (7b) and (7c) with the foregoing two equations for the additional terms of $\dot{\alpha}$ and $\dot{\beta}$ yields:

$$\dot{\alpha} = \langle L \rangle \bar{\alpha} + \dot{\alpha}_f = \langle L \rangle (\bar{\alpha} + \bar{\alpha}_f) = \langle L \rangle \bar{\alpha}^* \Rightarrow \bar{\alpha}^* = \bar{\alpha} + \frac{\bar{S}_f}{S_f}\alpha \tag{15a}$$

$$\dot{\beta} = \langle L \rangle \bar{\beta} + \dot{\beta}_f = \langle L \rangle (\bar{\beta} + \bar{\beta}_f) = \langle L \rangle \bar{\beta}^* \Rightarrow \bar{\beta}^* = \bar{\beta} + \frac{\bar{S}_f}{S_f}\beta \tag{15b}$$

With the N^* evolving according to Equation (11b), contrary to the fixed value of N for the unstructured soil, and β evolving according to Equation (15b), the consistency condition $\dot{f} = 0$ yields for the plastic modulus K_p instead of Equation (8b) the expression

$$K_p = -\left(\frac{\partial f}{\partial p_0^*} \bar{p}_0^* + \frac{\partial f}{\partial N^*} \bar{N}^* + \frac{\partial f}{\partial \beta} \bar{\beta}^* \right) \tag{16}$$

where $\bar{p}_0^*$, $\bar{N}^*$, and $\bar{\beta}^*$ are given above in Equations (12a), (12b) and (15b).

The incorporation of destructuration in a given model of the general framework provided by Equations (1)–(8b) results into the substitution of M^*, N^*, and p_0^* for M, N, and p_0, respectively,

DOI: 10.1002/nag

in various quantities entering the constitutive equations associated with the above formulation, for example, the $\bar{p}_0$, $\bar{\beta}$, $\bar{\alpha}$, $\partial f/\mathrm{d}p$, $\partial g/\mathrm{d}p$, $f=0$, $g=0$, etc, with *one exception:* in the corresponding equation for $\bar{p}_0$ (e.g. Equation (45)), which enters Equation (12a) and will depend on the specific hardening law used, while the M^*, N^* must substitute for M, N as said, the p_0^* must *not* substitute for the p_0 (which equals p_0^*/S_i). This is because the rate of p_0, which is in fact the basis for the definition of the quantity $\bar{p}_0$ according to Equation (7a), must be related to the plastic strain rates associated with the current structured state that is defined in terms of M^*, N^* in lieu of M, N. On the other hand, the rate of p_0 is related to p_0 itself and not to p_0^*, because the evolution of p_0^* has been already taken into account by the two terms of Equation (11a). Also one must not forget that the bounds in the hardening relations for β and α are now expressed in terms of N^* and M^*, consistent with the above substitutions.

2.1.3. Determination of $\bar{S}_i$ and $\bar{S}_f$. A link between the plastic strain rates and a measure of destructuration rate must now be established, since the former cause the latter. To this extent, the following previous suggestions in the literature [32, 33, 38–40] , an auxiliary internal variable called the destructuration plastic strain rate, $\dot{\varepsilon}_d^p$, is defined by

$$\dot{\varepsilon}_d^p = \sqrt{(1-A)\dot{\varepsilon}_v^{p2} + A\dot{\varepsilon}_q^{p2}} = \langle L\rangle \bar{\varepsilon}_d^p \tag{17a}$$

$$\bar{\varepsilon}_d^p = \sqrt{(1-A)\left(\frac{\partial g}{\partial p}\right)^2 + A\left(\frac{\partial g}{\partial q}\right)^2} \tag{17b}$$

where A is a new material constant distributing the effect of volumetric and deviatoric plastic strain rates to the value of $\dot{\varepsilon}_d^p$. Referring to Equations (10a), (10b) in conjunction with Equations (17a), (17b) one can propose a specific form of evolution equation for the S_i and S_f which reads

$$\begin{aligned} \dot{S}_i &= -k_i\left(\frac{1+e}{\lambda-\kappa}\right)(S_i-1)\dot{\varepsilon}_d^p = -\langle L\rangle k_i\left(\frac{1+e}{\lambda-\kappa}\right)(S_i-1)\bar{\varepsilon}_d^p = \langle L\rangle \bar{S}_i \\ &\Rightarrow \bar{S}_i = -k_i\left(\frac{1+e}{\lambda-\kappa}\right)(S_i-1)\bar{\varepsilon}_d^p \end{aligned} \tag{18a}$$

$$\begin{aligned} \dot{S}_f &= -k_f\left(\frac{1+e}{\lambda-\kappa}\right)(S_f-1)\dot{\varepsilon}_d^p = -\langle L\rangle k_f\left(\frac{1+e}{\lambda-\kappa}\right)(S_f-1)\bar{\varepsilon}_d^p = \langle L\rangle \bar{S}_f \\ &\Rightarrow \bar{S}_f = -k_f\left(\frac{1+e}{\lambda-\kappa}\right)(S_f-1)\bar{\varepsilon}_d^p \end{aligned} \tag{18b}$$

where e is the void ratio and the term $(1+e)/(\lambda-\kappa)$ is introduced only for convenience because it appears later in the evolution equation of p_0, where also the constants λ and κ are defined, while notice the fact that $\bar{S}_i$ and $\bar{S}_f$ are negative as they should. The specific form of the rate equations

DOI: 10.1002/nag

allows their integration yielding

$$S_i = 1 + (S_{i0} - 1) \exp\left(\frac{-k_i (1+e) \varepsilon_d^p}{\lambda - \kappa} \right) \tag{19a}$$

$$S_f = 1 + (S_{f0} - 1) \exp\left(\frac{-k_f (1+e) \varepsilon_d^p}{\lambda - \kappa} \right) \tag{19b}$$

Note that in the above integration the void ratio e is considered constant, as it happens under undrained loading. Of course it is conceivable that other forms of the rate equation for the S_i and S_f, not necessarily integrable, can also be used. With $\bar{S}_i$, $\bar{S}_f$, and $\bar{\varepsilon}_d^p$, known from above, the destructuration formulation is *complete*. New *model constants* addressing the destructuration constitutive ingredient are the k_i, k_f, and A ($=\frac{1}{2}$ default), and new *initial values* are S_{i0} and S_{f0}.

2.2. Formulation in the multiaxial space

In multiaxial stress and strain space all second-order tensors will be denoted by bold face. The stress tensor $\boldsymbol{\sigma}$ can be analyzed in a hydrostatic $p\mathbf{I}$ and a deviatoric component $\mathbf{s}$, defined by

$$p = (\mathrm{tr}\,\boldsymbol{\sigma})/3, \quad \mathbf{s} = \boldsymbol{\sigma} - p\mathbf{I} \tag{20}$$

where *tr* means the trace, and $\mathbf{I}$ is the identity tensor. The strain tensor $\boldsymbol{\varepsilon}$ is similarly decomposed in a volumetric ε_v and a deviatoric component $\mathbf{e}$ defined as

$$\varepsilon_v = \mathrm{tr}\,\boldsymbol{\varepsilon}, \quad \mathbf{e} = \boldsymbol{\varepsilon} - \varepsilon_v(\mathbf{I}/3) \tag{21}$$

A systematic multiaxial generalization of the triaxial constitutive relations is based on the following observation. In the triaxial setting any deviatoric tensor $\mathbf{x}$ develops only normal components x_i $(i = 1, 2, 3)$ with $tr\,\mathbf{x} = 0$, which means $x_2 = x_3 = (\frac{-1}{2})x_1$. It is straight forward to show that the following relation holds true:

$$\tfrac{3}{2}\mathbf{x} : \mathbf{x} = (x_1 - x_3)^2 = (\tfrac{3}{2}x_1)^2 = x^2 \tag{22}$$

where the symbol : implies the trace of the product of two adjacent tensors in which case $\mathbf{x} : \mathbf{x} = tr\mathbf{x}^2$, and where the triaxial counterpart x of $\mathbf{x}$ is introduced with the obvious association $(\frac{3}{2})x_1 = x$. For instance, substituting the deviatoric stress tensor $\mathbf{s}$ into Equation (22), one has $(\frac{3}{2})\mathbf{s} : \mathbf{s} = (s_1 - s_3)^2$, and knowing that $(s_1 - s_3) = (\sigma_1 - \sigma_3) = q$, the following relation between the deviatoric stress tensor $\mathbf{s}$ and its triaxial counterpart q is established:

$$\tfrac{3}{2}\mathbf{s} : \mathbf{s} = q^2 \tag{23}$$

Similarly, substituting the deviatoric strain tensor $\mathbf{e}$ into Equation (22), one obtains $(3/2)\mathbf{e} : \mathbf{e} = (e_1 - e_3)^2$, and knowing that $(e_1 - e_3) = (\varepsilon_1 - \varepsilon_3) = (\frac{3}{2})\varepsilon_q$, the following relation between the deviatoric strain tensor $\mathbf{e}$ and its triaxial counterpart ε_q is established:

$$\tfrac{2}{3}\mathbf{e} : \mathbf{e} = \varepsilon_q^2 \tag{24}$$

Notice the difference between the coefficients in Equations (23) and (24), which comes directly from the difference of the definitions for q and ε_q.

DOI: 10.1002/nag

2.2.1. Unstructured reference model. As usual, the strain tensor and its rate are decomposed into elastic and plastic parts, and so do the ε_v and $\mathbf{e}$ and their rates. The multiaxial generalization of the hypoelastic relations (3) is straightforward based on Equations (23) and (24) as

$$\dot{\boldsymbol{\varepsilon}}^e = \frac{\dot{\varepsilon}_v^e}{3}\mathbf{I} + \dot{\mathbf{e}}^e = \frac{\dot{p}}{3K}\mathbf{I} + \frac{\dot{\mathbf{s}}}{2G} \tag{25}$$

In the multiaxial space, the plastic strain rate $\dot{\boldsymbol{\varepsilon}}^p$ is given by the following flow rule:

$$\dot{\boldsymbol{\varepsilon}}^p = \langle L \rangle \frac{\partial g}{\partial \boldsymbol{\sigma}} \tag{26}$$

where g is the plastic potential, and L is the plastic loading index. The plastic potential and yield surface Equations (5) and (6) generalize as

$$g(\boldsymbol{\sigma}, \boldsymbol{\alpha}, p_\alpha, M) = 0 \tag{27}$$

$$f(\boldsymbol{\sigma}, \boldsymbol{\beta}, p_0, N) = 0 \tag{28}$$

where $\boldsymbol{\alpha}$ and $\boldsymbol{\beta}$ are deviatoric back stress-ratio tensors and serve as the multiaxial counterparts of the triaxial entities α and β, such that under triaxial conditions

$$\tfrac{3}{2}\boldsymbol{\alpha} : \boldsymbol{\alpha} = \alpha^2, \quad \tfrac{3}{2}\boldsymbol{\beta} : \boldsymbol{\beta} = \beta^2 \tag{29}$$

where $(3/2)\alpha_1 = \alpha$ and $(3/2)\beta_1 = \beta$ according to Equation (22). The rate equations for the internal variables are given by

$$\dot{p}_0 = \langle L \rangle \bar{p}_0 \tag{30a}$$

$$\dot{\boldsymbol{\alpha}} = \langle L \rangle \bar{\boldsymbol{\alpha}} \tag{30b}$$

$$\dot{\boldsymbol{\beta}} = \langle L \rangle \bar{\boldsymbol{\beta}} \tag{30c}$$

with proper generalization of the tensors $\bar{\boldsymbol{\alpha}}$ and $\bar{\boldsymbol{\beta}}$ from their triaxial counterparts $\bar{\alpha}$ and $\bar{\beta}$. Finally, the generalized determination of the loading index L is obtained by the consistency condition $\dot{f} = 0$ in conjunction with Equations (30a) and (30b) as

$$L = \frac{1}{K_p}\left(\frac{\partial f}{\partial \boldsymbol{\sigma}} : \dot{\boldsymbol{\sigma}}\right) = \frac{1}{K_p}\left(\frac{\partial f}{\partial \mathbf{s}} : \dot{\mathbf{s}} + \frac{\partial f}{\partial p} : \dot{p}\right) \tag{31a}$$

$$K_p = -\left(\frac{\partial f}{\partial p_0}\bar{p}_0 + \frac{\partial f}{\partial \boldsymbol{\beta}} : \bar{\boldsymbol{\beta}}\right) \tag{31b}$$

2.2.2. General approach to introduce structuration. As for the triaxial case, scalar isotropic and frictional destructuration factors S_i and S_f are introduced by Equations (9) and evolve according to Equations (10). A clarification is needed in generalizing Equations (11), because in the multiaxial case M can vary as a function of the stress state (via its dependence on Lode's angle to be introduced in Section 3.2.2). Therefore, in generalizing Equations 11 and 13, $\dot{M}^*$ and $\dot{N}^*$ are taken to represent the rate of change in M^* and N^*, respectively, due to destructuration only. Further $\boldsymbol{\alpha}$ and $\boldsymbol{\alpha}_f$ are now tensors, so the ratio $\boldsymbol{\alpha}_f/\boldsymbol{\alpha}$ in Equation (13) becomes the scalar by which alpha is

DOI: 10.1002/nag

multiplied to obtain $\boldsymbol{\alpha}_f$. The same applies to the tensors $\boldsymbol{\beta}$, $\boldsymbol{\beta}_f$. Proceeding in the same manner as for Equations (14) one then has

$$\bar{\alpha}_f = \frac{\bar{S}_f}{S_f}\alpha \Rightarrow \sqrt{\frac{3}{2}\bar{\boldsymbol{\alpha}}_f : \bar{\boldsymbol{\alpha}}_f} = \frac{\bar{S}_f}{S_f}\sqrt{\frac{3}{2}\boldsymbol{\alpha}:\boldsymbol{\alpha}} \Rightarrow \bar{\boldsymbol{\alpha}}_f = \frac{\bar{S}_f}{S_f}\boldsymbol{\alpha} \tag{32a}$$

$$\bar{\beta}_f = \frac{\bar{S}_f}{S_f}\beta \Rightarrow \sqrt{\frac{3}{2}\bar{\boldsymbol{\beta}}_f : \bar{\boldsymbol{\beta}}_f} = \frac{\bar{S}_f}{S_f}\sqrt{\frac{3}{2}\boldsymbol{\beta}:\boldsymbol{\beta}} \Rightarrow \bar{\boldsymbol{\beta}}_f = \frac{\bar{S}_f}{S_f}\boldsymbol{\beta} \tag{32b}$$

where $\sqrt{(\frac{3}{2})\bar{\boldsymbol{\alpha}}_f : \bar{\boldsymbol{\alpha}}_f} = \bar{\alpha}_f$ and $\sqrt{(\frac{3}{2})\bar{\boldsymbol{\beta}}_f : \bar{\boldsymbol{\beta}}_f} = \bar{\beta}_f$ are the scalar magnitudes of the tensors $\bar{\boldsymbol{\alpha}}_f$ and $\bar{\boldsymbol{\beta}}_f$, respectively, in the same manner as q is the scalar magnitude of the deviatoric stress tensor $\mathbf{s}$ in Equation (23). Generalization of Equations (15a) and (15b) follows as:

$$\dot{\boldsymbol{\alpha}} = \langle L\rangle\bar{\boldsymbol{\alpha}} + \dot{\boldsymbol{\alpha}}_f = \langle L\rangle(\bar{\boldsymbol{\alpha}} + \bar{\boldsymbol{\alpha}}_f) = \langle L\rangle\bar{\boldsymbol{\alpha}}^* \Rightarrow \bar{\boldsymbol{\alpha}}^* = \bar{\boldsymbol{\alpha}} + \frac{\bar{S}_f}{S_f}\boldsymbol{\alpha} \tag{33a}$$

$$\dot{\boldsymbol{\beta}} = \langle L\rangle\bar{\boldsymbol{\beta}} + \dot{\boldsymbol{\beta}}_f = \langle L\rangle(\bar{\boldsymbol{\beta}} + \bar{\boldsymbol{\beta}}_f) = \langle L\rangle\bar{\boldsymbol{\beta}}^* \Rightarrow \bar{\boldsymbol{\beta}}^* = \bar{\boldsymbol{\beta}} + \frac{\bar{S}_f}{S_f}\boldsymbol{\beta} \tag{33b}$$

Finally, the generalized form of Equation (16) for the plastic modulus becomes

$$K_p = -\left(\frac{\partial f}{\partial p_0^*}\bar{p}_0^* + \frac{\partial f}{\partial N^*}\bar{N}^* + \frac{\partial f}{\partial \boldsymbol{\beta}} : \bar{\boldsymbol{\beta}}^*\right) \tag{34}$$

where $\bar{p}_0^*$, $\bar{N}^*$, and $\bar{\boldsymbol{\beta}}^*$ are given by Equations (12a), (12b), and (15b), respectively.

2.2.3. Determination of $\bar{S}_i$ and $\bar{S}_f$. For the application of the proposed destructuration mechanism in the multiaxial stress/strain space, an equivalent generalized expression for the destructuration plastic strain rate is needed. The deviatoric strain tensor $\mathbf{e}$ and its triaxial counterpart ε_q are related by $(2/3)\mathbf{e}:\mathbf{e} = \varepsilon_q^2$ according to Equation (24), therefore, the multiaxial expression of the $\dot{\varepsilon}_d^p$ is as follows:

$$\dot{\varepsilon}_d^p = \langle L\rangle\bar{\varepsilon}_d^p = \sqrt{(1-A)\dot{\varepsilon}_v^{p2} + A(\tfrac{2}{3}\dot{\mathbf{e}}^p : \dot{\mathbf{e}}^p)} \tag{35}$$

where

$$\dot{\varepsilon}_v^p = \mathrm{tr}\dot{\boldsymbol{\varepsilon}}^p = \langle L\rangle \mathrm{tr}\left(\frac{\partial g}{\partial \boldsymbol{\sigma}}\right) \tag{36a}$$

$$\dot{\mathbf{e}}^p = \dot{\boldsymbol{\varepsilon}}^p - \frac{1}{3}\dot{\varepsilon}_v^p\mathbf{I} = \langle L\rangle\left[\frac{\partial g}{\partial \boldsymbol{\sigma}} - \frac{1}{3}\mathrm{tr}\left(\frac{\partial g}{\partial \boldsymbol{\sigma}}\right)\mathbf{I}\right] \tag{36b}$$

and the form of $\bar{\varepsilon}_d^p$ in multiaxial setting can easily be derived based on Equations (35), (36a) and (36b). With this generalized expression for $\bar{\varepsilon}_d^p$, the terms $\bar{S}_i$ and $\bar{S}_f$ are given again from Equations (18a) and (18b) and the formulation in the multiaxial space is complete.

DOI: 10.1002/nag

3. THE SANICLAY MODEL WITH DESTRUCTURATION

The presentation of the combined isotropic and frictional destructuration modeling is generic, in the sense that it can be incorporated in various elastoplastic soil constitutive models that fall within the general framework of the formulation by specifying, for example, forms of the yield and plastic potential surfaces (in lieu of the latter one needs only to specify the flow rule by other means) and rate evolution equations for the internal variables.

In order to illustrate the application of the presented constitutive ingredient for simulation of destructuration, the clay model by Dafalias *et al.* [15] is selected as a candidate. In addition to accounting for the destructuration, the model has a number of additional enhancements from its previous formulation in [15], namely:

1. The current void ratio e is used instead of the initial void ratio e_{in} wherever the latter appears in the formulation.
2. The N, and consequently the yield surface expression, is made function of the Lode angle, thus, N can be different in triaxial compression and extension.
3. The redefinition of the bounds for the evolving back stress ratios α and β in order to avoid a possible mathematical pitfall due to the Lode angle dependence.

3.1. The structured clay model in the triaxial space

The new formulation of the model is first presented in triaxial stress–strain space. The stress ratio η is defined by $\eta = q/p$.

3.1.1. Elastic relations. The hypoelastic relations given by Equation (3) are adopted where the elastic bulk and shear moduli K and G, respectively, are obtained from

$$K = \frac{p(1+e)}{\kappa}, \quad G = \frac{3K(1-2\nu)}{2(1+\nu)} \tag{37}$$

in which p and e are the *current* confining pressure and void ratio, respectively, κ the slope of the rebound line in the $e - \ln p$ space, and ν the constant Poisson's ratio.

3.1.2. Flow rule. The corresponding equations for the volumetric and deviatoric plastic strain rates are given by the flow rule of Equation (4) where the plastic potential $g = 0$ of Equation (5) for the structured clay can be found by substituting M^* for M in the plastic potential of Dafalias [6] which yields

$$g = (q - p\alpha)^2 - (M^{*2} - \alpha^2)\, p(p_\alpha - p) = 0 \tag{38}$$

with

$$M^* = S_f M; \begin{cases} M = M_c & \text{for } \eta > \alpha \\ M = M_e & \text{for } \eta < \alpha \end{cases} \tag{39}$$

and where α is the stress anisotropy variable, introducing the coupling of deviatoric and volumetric plastic strain rates in the plastic work expression postulated in Dafalias [6], M_c and M_e are the values of the critical state stress ratio M in compression and extension, respectively, and $m = M_e/M_c$ for future reference. The p_α is the value of p at $\eta = \alpha$, and can be obtained by solving

DOI: 10.1002/nag

for it from $g=0$ if desired. Clearly, one must have $|\alpha|<M$ for real-valued p and q in Equation (38). The plastic potential gradient components used in (4) are given by

$$\frac{\partial g}{\partial p}=p(M^{*2}-\eta^2), \quad \frac{\partial g}{\partial q}=2p(\eta-\alpha) \tag{40}$$

3.1.3. Yield surface. By substituting p_0^* and N^* for p_0 and N in the yield surface/plastic potential expression of Dafalias [6] in order to account for destructuration, and β for α in order to distinguish the rotational hardenings of the yield and plastic potential surfaces, the yield surface $f=0$ of Equation (6) for the structured clay is given by

$$f=(q-p\beta)^2-(N^{*2}-\beta^2)p(p_0^*-p)=0 \tag{41}$$

with

$$p_0^*=S_i p_0 \tag{42}$$

$$N^*=S_f N, \quad \begin{cases} N=N_c & \text{for } \eta>\alpha \\ N=N_e & \text{for } \eta<\alpha \end{cases} \tag{43}$$

The N, similar in nature to M, is defined by its values N_c and N_e in compression and extension, and $n=N_e/N_c$ for future reference. Clearly, one must have $|\beta|<M$ for real-valued p and q in Equation (41). The yield surface gradient components are given by

$$\frac{\partial f}{\partial p}=p(N^{*2}-\eta^2), \quad \frac{\partial f}{\partial q}=2p(\eta-\beta) \tag{44}$$

3.1.4. Hardening rules. The evolution laws for the structuration factors S_i and S_f are given by the generic Equations (18a), (18b) in the section for the general development of desructuration. It remains to define the specific evolution laws for p_0, α, and β, which in conjunction with those of S_i and S_f will define the evolution for the p_0^*, M^*, and N^*. For p_0 the classical evolution law in conjunction with Equation (40) for the volumetric plastic strain rate of the structured clay yields:

$$\dot{p}_0=\langle L\rangle\left(\frac{1+e}{\lambda-\kappa}\right)p_0\frac{\partial g}{\partial p}=\langle L\rangle\left(\frac{1+e}{\lambda-\kappa}\right)p_0 p(M^{*2}-\eta^2)=\langle L\rangle\bar{p}_0 \tag{45}$$

where the definition of $\bar{p}_0$ is self-evident. Notice that according to the observations and explanations given after Equation (16), the p_0 instead of p_0^* and the M^* instead of M appears in the above expression for $\bar{p}_0$. With this value of $\bar{p}_0$, use of Equations (11a)–(11c) and (12a)–(12c) in conjunction with Equations (18a) and (18b), which define the $\bar{S}_i$ and $\bar{S}_f$, provides the evolution laws for p_0^*, M^*, and N^*.

The evolution laws for α and β are given by Equations (14a) and (14b) and each one includes two components. The first component, $\bar{\alpha}$ or $\bar{\beta}$, is as proposed in Dafalias *et al.* [15] while the second component, $\bar{\alpha}_f$ or $\bar{\beta}_f$, which is adopted for inclusion of the frictional destructuration, is

DOI: 10.1002/nag

defined in Equations (15a) and (15b). Thus, referring also to Dafalias *et al.* [15] one has

$$\dot{\alpha} = \langle L \rangle (\bar{\alpha} + \bar{\alpha}_f) = \langle L \rangle \bar{\alpha}^* = \langle L \rangle \left[\left(\frac{1+e}{\lambda - \kappa} \right) C \left(\frac{p}{p_0^*} \right)^2 \left| \frac{\partial g}{\partial p} \right| |\eta - x_\alpha \alpha| (\alpha^b - \alpha) + \frac{\bar{S}_f}{S_f} \alpha \right] \tag{46}$$

$$\dot{\beta} = \langle L \rangle (\bar{\beta} + \bar{\beta}_f) = \langle L \rangle \bar{\beta}^* = \langle L \rangle \left[\left(\frac{1+e}{\lambda - \kappa} \right) C \left(\frac{p}{p_0^*} \right)^2 \left| \frac{\partial g}{\partial p} \right| |\eta - x_\beta \beta| (\beta^b - \beta) + \frac{\bar{S}_f}{S_f} \beta \right] \tag{47}$$

where the definition of $\bar{\alpha}^*$ and $\bar{\beta}^*$ is evident, C and x_α, x_β (both $\geqslant 1$) are model constants, and the term involving e, λ, and κ is introduced only for the convenience of similarity with the corresponding term in Equation (45). The term x_β will have the default value of 1, but it is left as x_β in Equation (47) in order to facilitate in the sequel the simplification of the model to one with a single surface. The value $x_\beta = 1$ yields an expression for $\bar{\beta}$ as in [15]. The various terms associated with $\bar{\alpha}$ or $\bar{\beta}$ and their explanation can be found in [15]. A difference with the foregoing reference concerns the values of the bounds α^b and β^b in the above equations, which are defined here as

$$\begin{aligned} \alpha^b &= M_e^* = S_f M_e \qquad \text{for } \eta / x_\alpha > \alpha \\ \alpha^b &= -M_e^* = -S_f M_e \quad \text{for } \eta / x_\alpha < \alpha \end{aligned} \tag{48}$$

and

$$\begin{aligned} \beta^b &= N_e^* = S_f N_e \qquad \text{for } \eta / x_\beta > \beta \\ \beta^b &= -N_e^* = -S_f N_e \quad \text{for } \eta / x_\beta < \beta \end{aligned} \tag{49}$$

Equations (48) and (49) are modified compared with the similar equations in Dafalias *et al.* [15] (where the rational behind the definition of the bounds is developed in detail) in two respects. The first is the obvious use of the structured values M_e^* and N_e^* instead of M_e and N_e, consistent with the observations following Equation (16). The second is that the bounds are expressed in terms of the extension values M_e and N_e for both compression and extension loading, while in [15] each bound was associated with the corresponding values of M and N in compression or extension. This is done here in order to avoid the following situation. Assume that, for example, we load at very high η values in which case the α would approach the bound M_c, which exceeds the M_e. This might create problems if one decides then to change from compression to extension because $|\alpha| > M_e$! This is not likely to happen because in very high values of η the yield surface begins to shrink very fast due to dilation and we reach the critical state before we have the evolution of α toward its bound M_c. But in order to avoid even a minute possibility for such a situation to arise, the bounds are set using the smaller M_e for either compression or extension. The same applies for the bounds of β. Such a modification has insignificant effect on the simulative capability of the model, while it guarantees avoidance of mathematical problems.

3.1.5. Loading index and plastic modulus. For the completion of the model, the determination of the loading index L is required. The L is given by Equation (8a) of the generic development with the components of the gradient of $f = 0$ given above by Equations (44). As the destructuration is included, the corresponding plastic modulus is now given by Equation (16) rather than Equation (8b), where the $\bar{p}_0^*$, $\bar{N}^*$, and $\bar{\beta}^*$ are defined by Equations (12a), (12b), and (15b),

DOI: 10.1002/nag

respectively, in conjunction with Equations (45), (18a), and (18b) which define the $\bar{p}_0$, $\bar{S}_i$ and $\bar{S}_f$, and the derivatives:

$$\frac{\partial f}{\partial p_0^*}=-p(N^{*2}-\beta^2),\quad \frac{\partial f}{\partial N^*}=-2p(p_0^*-p)N^*,\quad \frac{\partial f}{\partial \beta}=-2p(q-p_0^*\beta) \tag{50}$$

3.2. The structured clay model in the multiaxial space

Following the general rules presented in Equations (23) and (24), the generalization of the triaxial formulation to the multiaxial stress space is presented in this section. In the following equations the stress ratio tensor $\mathbf{r}$ is defined by $\mathbf{r}=\mathbf{s}/p$, and serves as the the multiaxial counterpart of the triaxial entity $\eta=q/p$, such that according to Equation (23) one has

$$\tfrac{3}{2}\mathbf{r}:\mathbf{r}=\eta^2 \tag{51}$$

3.2.1. Elastic relations. The hypoelastic Equations (25) of the generic formulation are adopted with K and G given by Equation (37) of the triaxial formulation.

3.2.2. Flow rule. The corresponding equation for the plastic strain rate in multiaxial space is given by the flow rule of Equation (26). Based on Equations (23) and $(29)_1$, the analytical expression 38 of the plastic potential generalizes to

$$g=\tfrac{3}{2}(\mathbf{s}-p\boldsymbol{\alpha}):(\mathbf{s}-p\boldsymbol{\alpha})-(M^{*2}-\tfrac{3}{2}\boldsymbol{\alpha}:\boldsymbol{\alpha})p(p_\alpha-p)=0 \tag{52}$$

with $M^*=S_fM$ according to Equation (9c) of the generic formulation. Recall that the critical state stress-ratio M in Equation (38) acquires different values M_c and $M_e=mM_c$ according to the sign of $\eta-\alpha$ as explained in Equation (39). The M in the multiaxial stress space will be interpolated between its values M_c and mM_c by means of a Lode angle θ_α, as already presented in [15] according to the proposition by Argyris *et al.* [41], which reads as

$$M=\Theta(\theta_\alpha,m)M_c=\frac{2m}{(1+m)-(1-m)\cos 3\theta_\alpha}M_c \tag{53}$$

$$\cos 3\theta_\alpha=\sqrt{6}\,\mathrm{tr}\,\mathbf{n}_\alpha^3,\quad \mathbf{n}_\alpha=\frac{\mathbf{r}/x_\alpha-\boldsymbol{\alpha}}{[(\mathbf{r}/x_\alpha-\boldsymbol{\alpha}):(\mathbf{r}/x_\alpha-\boldsymbol{\alpha})]^{1/2}} \tag{54}$$

The gradient of g is calculated based on Equations (52)–(54), similar to what was presented in Equations (18) of [15], as

$$\frac{\partial g}{\partial \boldsymbol{\sigma}}=3\,(\mathbf{s}-p\boldsymbol{\alpha})+\frac{1}{3}p\left(M^{*2}-\frac{3}{2}\mathbf{r}:\mathbf{r}\right)\mathbf{I}+\frac{\partial g}{\partial \theta_\alpha}\frac{\partial \theta_\alpha}{\partial \boldsymbol{\sigma}} \tag{55}$$

with

$$\frac{\partial g}{\partial \theta_\alpha}=6M^{*2}p(p_\alpha-p)\left(\frac{1-m}{2m}\right)\Theta(\theta_\alpha,m)\sin 3\theta_\alpha \tag{56}$$

$$\frac{\partial \theta_\alpha}{\partial \boldsymbol{\sigma}}=\frac{-3[\mathbf{n}_\alpha^2-(\mathrm{tr}\,\mathbf{n}_\alpha^3)\mathbf{n}_\alpha-\frac{1}{3}\mathbf{I}(1+\mathrm{tr}(\mathbf{n}_\alpha^2\boldsymbol{\alpha})-\mathrm{tr}\,\mathbf{n}_\alpha^3\mathrm{tr}(\mathbf{n}_\alpha\boldsymbol{\alpha}))]}{p[(3/2)(\mathbf{r}-\boldsymbol{\alpha}):(\mathbf{r}-\boldsymbol{\alpha})]^{1/2}(1-6\,\mathrm{tr}^2\,\mathbf{n}_\alpha^3)^{1/2}} \tag{57}$$

The p_α is the value of p at $\mathbf{s}=p\boldsymbol{\alpha}$, and can easily be obtained by solving for it from $g=0$.

DOI: 10.1002/nag

3.2.3. Yield surface. Similarly, the generalization of Equation (41) for the yield surface is based on Equations (23) and $(29)_1$ and yields

$$f=\tfrac{3}{2}(\mathbf{s}-p\boldsymbol{\beta}):(\mathbf{s}-p\boldsymbol{\beta})-(N^{*2}-\tfrac{3}{2}\boldsymbol{\beta}:\boldsymbol{\beta})\,p(p_0^*-p)=0 \tag{58}$$

with $p_0^*=S_i\,p_0$ and $N^*=S_f N$ according to Equations (9a) and (9b) of the generic formulation. Similar to M of Equation (52) for the plastic potential, the N acquires different values of N_c and $N_e=nN_c$ according to the sign of $\eta-\beta$ as explained in Equation (43). Interpolation of the N in the multiaxial stress space between its values N_c and nN_c is done by means of another Lode angle θ_β as

$$N=\Theta(\theta_\beta,n)N_c=\frac{2n}{(1+n)-(1-n)\cos 3\theta_\beta}N_c \tag{59}$$

$$\cos 3\theta_\beta=\sqrt{6}\,\mathrm{tr}\mathbf{n}_\beta^3,\quad \mathbf{n}_\beta=\frac{(\mathbf{r}/x_\beta)-\boldsymbol{\beta}}{[((\mathbf{r}/x_\beta)-\boldsymbol{\beta}):((\mathbf{r}/x_\beta)-\boldsymbol{\beta})]^{1/2}} \tag{60}$$

Observe that by setting $n=1$, the value of interpolation function $\Theta(\theta_\beta,n)$ will be equal to 1 regardless of the value of the Lode angle θ_β, which changes this part of the formulation back to its original form in [15]. The gradient of $f=0$ is given by

$$\frac{\partial f}{\partial\boldsymbol{\sigma}}=3(\mathbf{s}-p\boldsymbol{\beta})+\frac{1}{3}p\left(N^{*2}-\frac{3}{2}\mathbf{r}:\mathbf{r}\right)\mathbf{I}+\frac{\partial f}{\partial\theta_\beta}\frac{\partial\theta_\beta}{\partial\boldsymbol{\sigma}} \tag{61}$$

with

$$\frac{\partial f}{\partial\theta_\beta}=6N^{*2}p(p_0^*-p)\left(\frac{1-n}{2n}\right)\Theta(\theta,n)\sin 3\theta_\beta \tag{62}$$

$$\frac{\partial\theta_\beta}{\partial\boldsymbol{\sigma}}=\frac{-3[\mathbf{n}_\beta^2-(\mathrm{tr}\,\mathbf{n}_\beta^3)\mathbf{n}_\beta-\frac{1}{3}\mathbf{I}(1+\mathrm{tr}(\mathbf{n}_\beta^2\boldsymbol{\beta})-\mathrm{tr}\,\mathbf{n}_\beta^3\mathrm{tr}(\mathbf{n}_\beta\boldsymbol{\beta}))]}{p[(3/2)(\mathbf{r}-\boldsymbol{\beta}):(\mathbf{r}-\boldsymbol{\beta})]^{1/2}(1-6\,\mathrm{tr}^2\,\mathbf{n}_\beta^3)^{1/2}} \tag{63}$$

3.2.4. Hardening rules. The rate equations of evolution of the internal variables S_i, S_f, p_0, $\boldsymbol{\alpha}$, and $\boldsymbol{\beta}$ must be determined which, in turn, will define the evolution for the p_0^*, M^*, and N^*. The evolution laws for the structuration factors S_i and S_f are given by the generic Equations (18a) and (18b) of the section for the general development of desructuration, as they were for the triaxial space. The generalized form of the expressions for $\dot{\varepsilon}_d^p$ and $\bar{\varepsilon}_d^p$ has been already presented in Equations (35)–(35), of the generic multiaxial formulation. For the p_0, the same equation as Equation (45) in the triaxial is assumed, whereby rephrasing the expression for $\dot{\varepsilon}_v^p$ based on Equation (36a) one has

$$\dot{p}_0=\langle L\rangle\left(\frac{1+e}{\lambda-\kappa}\right)p_0\mathrm{tr}\left(\frac{\partial g}{\partial\boldsymbol{\sigma}}\right)=\langle L\rangle\bar{p}_0 \tag{64}$$

where the definition of $\bar{p}_0$ is evident. With this value of $\bar{p}_0$, use of Equations (11a)–(12c) in conjunction with Equations (18a) and (18b) which define the $\bar{S}_i$ and $\bar{S}_f$ provide the evolution laws for p_0^*, M^*, and N^*.

DOI: 10.1002/nag

The evolution laws for $\boldsymbol{\alpha}$ and $\boldsymbol{\beta}$ are given by Equations (15a) and (15b) of the generic multiaxial formulation and each one includes two components. The first component, $\bar{\alpha}$ or $\bar{\beta}$, is as proposed in [15] while the second component, $\bar{\alpha}_f$ or $\bar{\beta}_f$, which is adopted for inclusion of the frictional destructuration, is defined in Equations (15a) and (15b). Thus, with reference to [15] one can write

$$\dot{\boldsymbol{\alpha}} = \langle L \rangle \left(\bar{\boldsymbol{\alpha}} + \bar{\boldsymbol{\alpha}}_f \right) = \langle L \rangle \bar{\boldsymbol{\alpha}}^*$$

$$= \langle L \rangle \left[\left(\frac{1+e}{\lambda - \kappa} \right) C \left(\frac{p}{p_0^*} \right)^2 \left| \operatorname{tr} \left(\frac{\partial g}{\partial \boldsymbol{\sigma}} \right) \right| \left[\frac{3}{2} (\mathbf{r} - x_\alpha \boldsymbol{\alpha}) : (\mathbf{r} - x_\alpha \boldsymbol{\alpha}) \right]^{1/2} (\boldsymbol{\alpha}^b - \boldsymbol{\alpha}) + \frac{\bar{S}_f}{S_f} \boldsymbol{\alpha} \right]$$

$$\dot{\boldsymbol{\beta}} = \langle L \rangle \left(\bar{\boldsymbol{\beta}} + \bar{\boldsymbol{\beta}}_f \right) = \langle L \rangle \bar{\boldsymbol{\beta}}^*$$

$$= \langle L \rangle \left[\left(\frac{1+e}{\lambda - \kappa} \right) C \left(\frac{p}{p_0^*} \right)^2 \left| \operatorname{tr} \left(\frac{\partial g}{\partial \boldsymbol{\sigma}} \right) \right| \left[\frac{3}{2} (\mathbf{r} - x_\beta \boldsymbol{\beta}) : (\mathbf{r} - x_\beta \boldsymbol{\beta}) \right]^{1/2} (\boldsymbol{\beta}^b - \boldsymbol{\beta}) + \frac{\bar{S}_f}{S_f} \boldsymbol{\beta} \right]$$

The generalization of Equations (48) and (49) for the bounds $\boldsymbol{\alpha}^b$ and $\boldsymbol{\beta}^b$ reads

$$\boldsymbol{\alpha}^b = \sqrt{\tfrac{2}{3}} S_f M_e \mathbf{n}_\alpha, \quad \boldsymbol{\beta}^b = \sqrt{\tfrac{2}{3}} S_f N_e \mathbf{n}_\beta \tag{65}$$

where $\mathbf{n}_\alpha$ is defined by Equation $(54)_2$ with $\mathbf{r}/x_\alpha$ substituting for $\mathbf{r}$ and $\mathbf{n}_\beta$ defined by Equation $(60)_2$. The various terms appearing as part of the first component $\bar{\boldsymbol{\alpha}}$ or $\bar{\boldsymbol{\beta}}$ are elaborated in [15]. The reason for the difference of the bounds defined above from those of [15] is explained along the same lines for the triaxial formulation.

3.2.5. Loading index and plastic modulus. From the consistency condition $\dot{f} = 0$ applied to Equation (58), one obtains Equations (8a) and (16) of the generic formulation for the loading index L and plastic modulus K_p, respectively, where the gradient $\partial f / \partial \boldsymbol{\sigma}$ is given by Equation (61), the $\bar{p}_0^*$, $\bar{N}^*$, and $\bar{\beta}^*$ are given by Equations (12a)–(12c) with $\bar{p}_0$ defined in Equation (45) and the derivatives entering Equation (16) for K_p given by

$$\frac{\partial f}{\partial p_0^*} = -p \left(N^{*2} - \frac{3}{2} \boldsymbol{\beta} : \boldsymbol{\beta} \right) \tag{66}$$

$$\frac{\partial f}{\partial N^*} = -2p(p_0^* - p) N^* \tag{67}$$

$$\frac{\partial f}{\partial \boldsymbol{\beta}} = -3p(\mathbf{s} - p\boldsymbol{\beta}) + 3p(p_0^* - p)\boldsymbol{\beta} \tag{68}$$

3.3. Illustration of the destructuration effect

Figure 2 illustrates the effects of isotropic and frictional destructuration mechanisms independently and in combination. In order to have a visual impression of the destructuration effect, undrained triaxial loading in compression and extension is simulated from a K_0 initial stress state assuming

DOI: 10.1002/nag

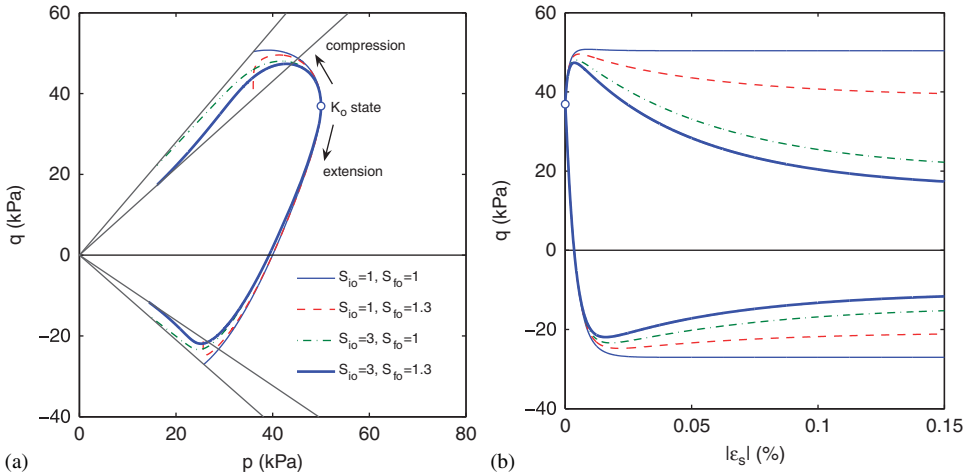

Figure 2. Illustration of the effects of isotropic and frictional destructuration mechanisms independently and in combination.

Table I. Constant of the SANICLAY model with destructuration for Bothkennar clay.

Parameter	Description	Value
$M_c(N_c)$	Slope of the CSL on the compression side of $p-q$ plane (shape of the yield surface)	1.4 (1.2)
$m(n)$	Ratio of the slope of the CSL on the extension and on the compression side of $p-q$ plane (shape of the yield surface)	0.75 (1)
ν	Poisson's ratio	0.2
λ	Total volume change due to a change in mean stress	0.255
κ	Elastic volume change due to a change in mean stress	0.03
$x_\alpha(x_\beta)$	Saturation limit of anisotropy under paths with $\eta=$ const.	3.14 (1)
C	Rate of evolution of anisotropy	12
k_i	Parameter describing the rate of isotropic destructuration	0.9
k_f	Parameter describing the rate of frictional destructuration	1.3
A	Parameter describing coupling between volumetric and frictional destructuration	0.2

that the structure is given by specific values of the structuration parameters S_i and S_f existing at the initiation of loading, which for our purpose constitute the initial values S_{i0} and S_{f0}. The initial values of p_0^* and M^* are kept the same in the simulations. The existence of S_i and S_f at values greater than one reflects the development of the structure over time for a soil sample *in-situ* under K_0 conditions. The values of various constants used are typical of a structured clay and are taken from Table I reflecting the values of a calibration procedure to be explained in the sequel for an actual clay. The plots of the undrained stress paths as well as the triaxial deviatoric stress–strain curves are shown in Figure 2. The runs are made with different combinations of values of S_{i0} and S_{f0}. Notice that according to Equations (18a) and (18b) the value of 1 for one of the S_{i0} or S_{f0} implies that the corresponding destructuration mechanism is inactive since there is no structure associated with it.

DOI: 10.1002/nag

Either one of the isotropic or frictional destructuration induces softening in the response and the combination of both the destructuration mechanisms induces the more intense softening, as expected. Given that the initial values of p_0^* and M^* are kept the same in different simulations, observe that the presence of only isotropic destructuration ($S_{f0}=1$) brings the final stress-ratio q/p to $M=M^*$, whereas the presence of the frictional destructuration ($S_{f0}>1$) brings the final stress ratio q/p to $M<M^*$. The above help in understanding the relative role each destructuration mechanism plays vis-a-vis the simulated clay response.

3.4. Special cases

The current presentation of the SANICLAY model gives the freedom to the user for choosing the level of complexity of the model formulation and to some extent the number of model parameters. In general, this model has a non-associative flow rule, that is, the plastic potential surface is different from the yield surface. The two surfaces have different back stress-ratios α and β, and bound values M and N. The most general form of the model is associated with all of the introduced features, that is, independent values for M, N, α, and β. The followings, however, are two special cases that can be attained from this versatile model formulation which look promising simpler alternatives.

3.4.1. Two surface model with $N=M$. The main reason for introducing an M different from N in the original SANICLAY model [15] was to capture softening without destructuration in undrained loading after a K_0 consolidation process for clays that did not exhibit destructuration characteristics; the resulting non-associative flow rule had also other advantages as to the more realistic simulation of the undrained stress path. Destructuration features allow us to capture such softening even with $M=N$. Of course the possibility of setting different M and N values gives freedom during calibration process for obtaining better match to the results, but in a boundary value problem one may prefer to save calibration of two parameters (N_c and n) by having $N=M$, which still leaves the two surfaces different because of different α and β. In the current formulation this is achieved by setting $N_c=M_c$ and $n=m$. This version of the model uses a unique bound for the rotational hardening of both the yield and plastic potential surfaces, that is, $N=M$. In this case softening, if any, can still be predicted not only in undrained but also in drained cases of loading using the embedded destructuration mechanism. Notice that for better simulation of the initial part of the undrained loading after oedometric consolidation the choice $x_\beta=1$ is made, which leads the $\boldsymbol{\beta}$ toward $\mathbf{r}$ under constant $\mathbf{r}$ loading.

Simulations with the destructuration mechanism show that it is actually possible *not* to have softening under drained loading for a structured sample, while having softening under undrained, thus, negating the argument presented in [15] that '*destructuration would have induced softening under both drained and undrained conditions*'. In other words, when one sees softening in undrained data and no softening in drained, as in the Lower Cromer Till (LCT) clay in data of Gens [42], he must *not* necessarily conclude that no destructuration exists.

3.4.2. One surface model (*associative flow rule*). By setting $N=M$ (i.e. $N_c=M_c$ and $n=m$) and $x_\beta=x_\alpha>1$, one obtains automatically a single surface version of the model which, apart from the destructuration constitutive ingredient, is in fact the original version proposed by Dafalias (1986) and is characterized by an associative flow rule and ensuing normality. Such simplification has clear advantages in large computational schemes to solve boundary-value problems, since (a) the single

DOI: 10.1002/nag

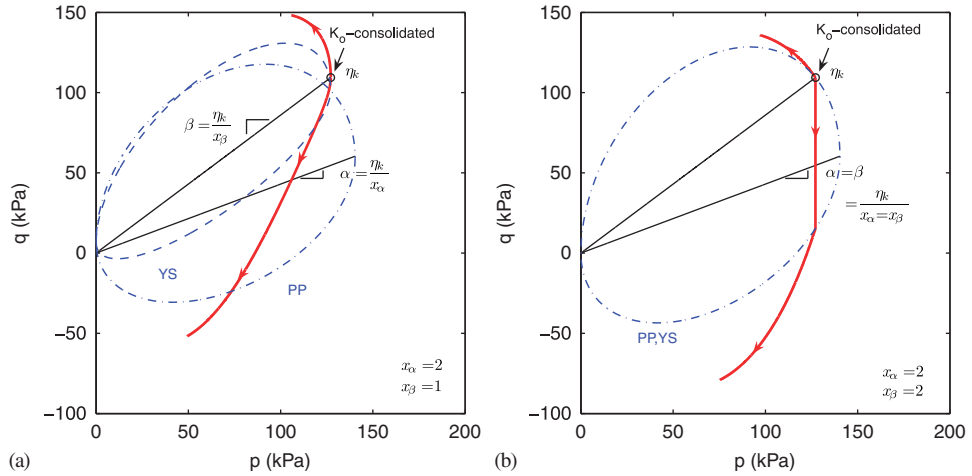

Figure 3. Effect of the choice of x_β on the undrained stress path of a K_0 consolidated sample: (a) two surface model with $N = M$; and (b) one surface model (YS: Yield Surface; PP: Plastic Potential).

surface version offers the symmetry of the elastoplastic stiffens matrix due to associative flow rule; (b) only one rotational back stress ratio needs to be updated. Nevertheless, the simplifications produce some serious drawbacks in the model's ability to reproduce real soil behavior, as illustrated in Figure 3 and further explained in what follows.

First, it is important to understand that the plastic potential *cannot* have a rotational back stress α that stabilizes at η_k, the stress ratio under K_0.[§] This is because K_0 loading must produce both volumetric *and* deviatoric plastic strains, which is not possible if the α is identical to η_k in which case only volumetric plastic strain is produced (the normal to the plastic potential is parallel to the p axis). In other words, one *must* have $x_\alpha > 1$ in the evolution law for α, so that $\alpha = \eta_k / x_\alpha$ at stabilization of rotation.

Then, as the choice of a single surface version implies necessarily $\alpha = \beta$, it means that also the yield surface will stabilize at $\alpha = \beta = \eta_k / x_\alpha$ under K_0. The negative consequence of this simplifying assumption is that upon undrained triaxial loading following K_0 the undrained stress path in compression will start with a steep slope to the left, instead of rising first vertically and then turning to the left as shown in the experiments. Moreover, the undrained stress path in extension after K_0 will first go down vertically inside the elastic domain, before it turns left again as it was supposed to do from the beginning. These drawbacks are shown in Figure 3. Avoidance of such a response was the reason to use two surfaces where $\alpha = \eta_k / x_\alpha$ with $x_\alpha > 1$ and $\beta = \eta_k$ with the choice $x_\beta = 1$ (see Figure 3).

On balance the choice between simplicity and accuracy of simulation belongs to the user's needs. The complexity associated with the Lode angle remains in the one-surface model, and the symmetry of the tangent stiffness matrix is not an issue if explicit time-integration is used in the solution of a boundary-value problem.

[§]This would happen if one sets $x_\alpha = 1$ in Equations (46) and (47) and considers the end of frictional destructuration when $S_f = 1$ and $\bar{S}_f = 0$.

DOI: 10.1002/nag

In the following the soil behavior will be simulated using all three versions, namely the general one, the one with $M=N$ but with different α and β and the single surface where $M=N$ and $\alpha=\beta$, providing a clear comparison.

4. MODEL CALIBRATION AND SIMULATIONS

4.1. Calibration of the model

The calibration will be done based on the most general form of the model, that is, using independent values for M, N, α, and β. The SANICLAY model with destructuration requires the calibration of 13 constants (see Table I). Three of these are the new model constants for simulation of destructuration (k_i, k_f, A). The parameter A could be set to 0.5 as a default value. Parameters N_c and n could be chosen same as M_c and m, respectively. If more accuracy is required one can also calibrate these three parameters accordingly. Finally, parameter x_β will be set equal to 1 for reasons explained earlier, unless one prefers to go with a single surface version and associative flow rule in which case $x_\beta = x_\alpha \geqslant 1$. The model constants associated with the original SANICLAY model can be calibrated based on the instructions given in [15]. Calibration of the destructuration parameters requires data from well-established laboratory tests on intact samples, namely:

- One-dimensional (K_0) or preferably isotropic consolidation tests to stresses beyond the destructuration limit using an oedometric or a triaxial device (for constant k_i and initial value of the state variable S_i).
- Undrained triaxial compression or extension tests on intact samples to strains beyond the destructuration limit (for constant k_f and initial value of the state variable S_f).

The mechanical response of *undisturbed* and *reconstituted* samples of Bothkennar clay have been studied by Smith *et al.* [21] and Allman and Atkinson [43], respectively. Gajo and Muir Wood [34] have proposed two constitutive models for natural and reconstituted clays. They have calibrated their models for the presented data by Smith *et al.* [21] and Allman and Atkinson [43]. In the current work, however, we focus on the structured clay and calibrate the present model for *undisturbed* Bothkennar clay to capture the presented experimental results in Smith *et al.* [21]. The material was taken with Laval and Sherbrooke samplers from depths of $5.3-6.2\,m$.

4.1.1. Parameters M_c, m, N_c (and Estimation of n). Figure 4(a) presents the behavior of Bothkennar clay in undrained compression and extension tests. In this figure points A, B, C, and D correspond to the *in-situ*, oedometrically consolidated, isotropically consolidated, and passively consolidated states of the soil sample, respectively, with cases B, C, and D started off with the same *in-situ* consolidation of case A. The data are presented in terms of effective stress path. Given these tests on Bothkennar clay, the M_c and $m=M_e/M_c$ are estimated directly from the effective stresses at the end of the tests as $M_c=1.4$ and $m=M_e/M_c\simeq 0.75$. Clearly, using $M_c=M_e=1.4$ in this case would seriously overestimate the strength in extension.

Figure 4(b) shows the corresponding yield surface for the model at point B for three different values of N_c^*. For a non-rotating or slowly rotating yield surface, the undrained stress path for triaxial compression almost follows the shape of the yield surface. Therefore, having the experimental results of undrained stress path for the triaxial compression test at point B lead to the estimation of $N_c^*=1.2$ for point B. This is already smaller than the value of $M_c=1.4$ and on the

DOI: 10.1002/nag

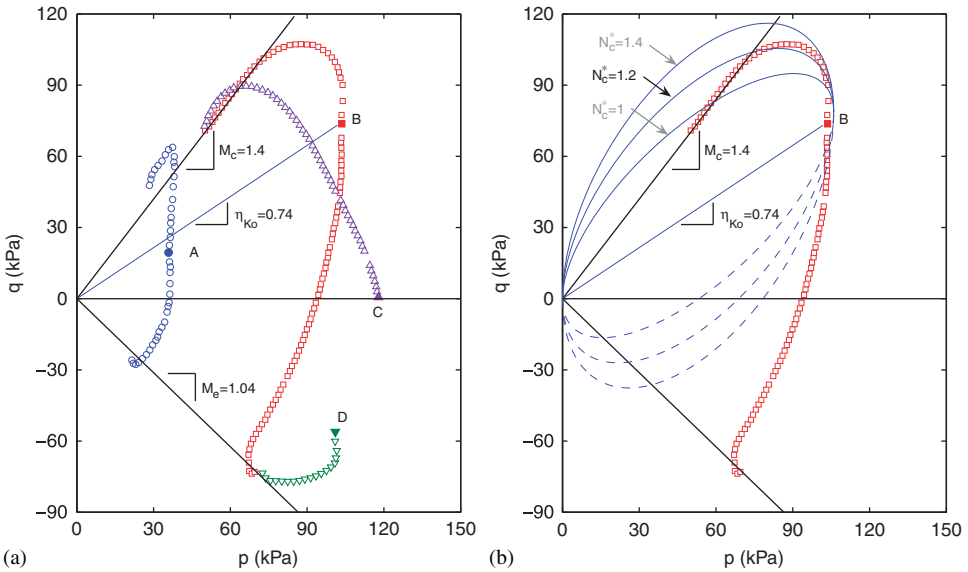

Figure 4. Calibration of constants M_c, $m = M_e/M_c$ and N_c^*.

other hand, the experimental results suggest that in this stress path there is not much of frictional destructuration after point B, which means that the frictional structuration factor S_f, if any, has been exhausted and reached its limit value of 1 during the one-dimensional compression path, which brought the state from point A to point B. Hence, it is a plausible assumption that at point B the sample has $S_f = 1$ and therefore $N_c = N_c^*/S_f = 1.2$. The value of n can be assumed to be the same as m but later fine tunning of the model parameters shows that for this clay a value of $n = 1$ gives better results.

4.1.2. Parameter ν. Poisson's ratio ν is calibrated based on results shown in Figure 5 for (elastic) K_0 unloading after K_0 consolidation on a reconstituted sample. This figure shows the stress paths followed during one-dimensional compression to $p = 200$ kPa and swelling to $p = 100$ kPa or 50 kPa. As an approximation, the initial part of the swelling path is proposed for use in calibration of the elastic Poison's ratio ν of the clay. Upon unloading from K_0 conditions the initial part of the stress path lies within the yield surface [15]. In such a path, the ratio of the elastic strain rates $\dot{\varepsilon}_v^e/\dot{\varepsilon}_q^e = \frac{3}{2}$, which gives $\dot{q}/\dot{p} = 2(1-2\nu)/(1+\nu)$. Comparison with the slope $\mathrm{d}q/\mathrm{d}p$ of the data from Figure 5, yields a value $\nu = 0.2$ for Bothkennar clay. Please note that the data belong to reconstituted Bothkennar clay [43], which we assume has approximately the same Poison's ratio as the intact sample of this clay.

4.1.3. Parameters κ and λ. The parameters κ and λ can be obtained from the results of isotropic or one-dimensional compression (CI or CK_0) presented in $e - \log p$ space. We use the data of oedometric consolidation test on reconstituted (unstructured) samples of Bothkennar clay (Intrinsic Compression Curve, ICC) in order to calibrate these parameters. Smith *et al.* [21] have presented their results in $e - \log \sigma_a$ space (Figure 6(a)) with no information about the horizontal stress, a

DOI: 10.1002/nag

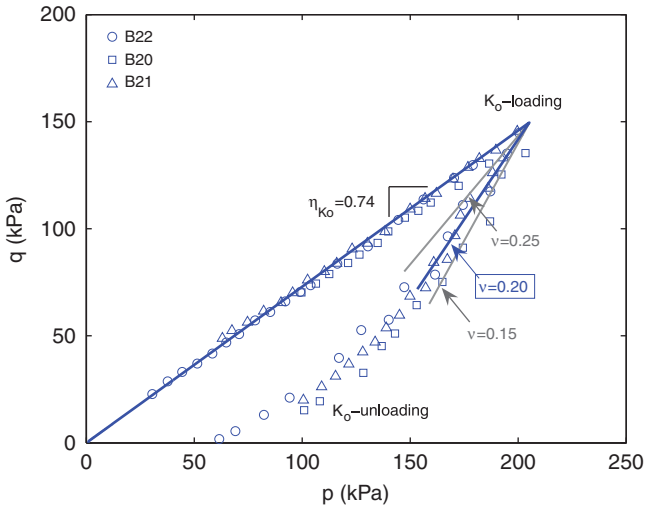

Figure 5. Calibration of constant v.

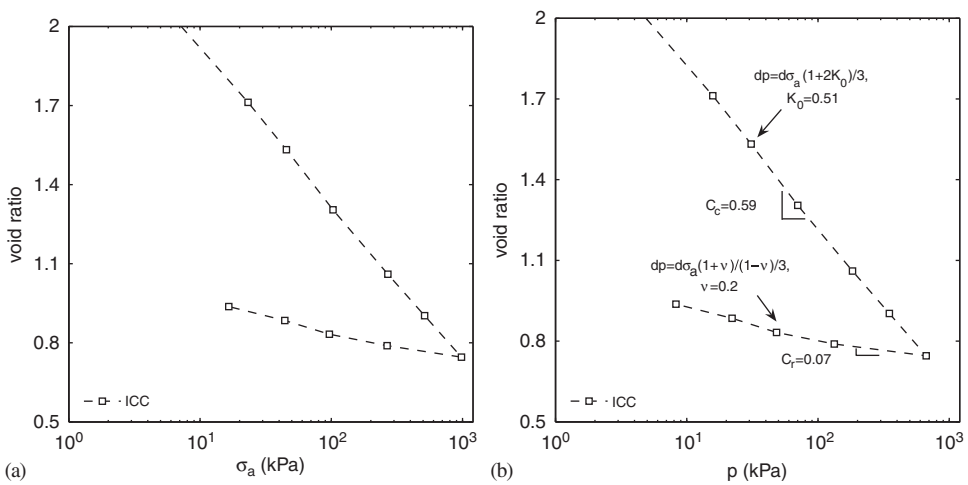

Figure 6. Calibration of constants κ and λ via C_r and C_c from oedometer tests on reconstituted samples.

typical type of results from many experimentalists. The procedure to obtain the corresponding plot in $e-\log p$ space (Figure 6(b)) is as follows.

Both Figures 4 and 5 show a value of $\eta_{ko}=0.74$ that defines the corresponding value of $K_0=(3-\eta_{k_0})/(2\eta_{k_0}+3)=0.52$. Assuming a constant K_0, for the loading part we have $\dot{p}=\dot{\sigma}_a(1+2K_0)/3$. The initial part of the unloading is elastic where we have $\dot{\varepsilon}_h=((1-v)\dot{\sigma}_h-v\dot{\sigma}_a)/E=0$ or $\dot{\sigma}_a=\dot{\sigma}_h(1-v)/v$, which implies that $\dot{p}=(\dot{\sigma}_a+2\dot{\sigma}_h)/3=(\dot{\sigma}_a/3)(1+v)/(1-v)$. Figure 6(b) is reproduced from Figure 6(a) using the above-mentioned relations for the loading and unloading

DOI: 10.1002/nag

parts. In other words, Figures 6(a), (b) show the results of oedometric consolidation in $e-\log\sigma_a$ and $e-\log p$ spaces, respectively.

Given that the model constants λ and κ are defined as slopes of the normal compression and swelling lines in $e-\ln p$ space, and knowing that these lines are parallel to the oedometric consolidation and swelling lines, the C_c and C_r slopes that are measured in Figure 6(b) are related to λ and κ as: $\lambda=C_c/\ln 10=0.255$ and $\kappa=C_r/\ln 10=0.03$.

4.1.4. Parameter x_α (and x_β). For the estimation of the constant x_α, the case of a drained path with $\eta=\eta_k=$constant is considered. In such a path eventually the two surfaces cease to rotate while the yield surface keeps expanding due to the increase of p_0^*. Then $\alpha=\alpha_k=\eta_k/x_\alpha$ and $\beta=\beta_k=\eta_k$ (since $x_\beta=1$) as it follows from Equations (46) and (47), respectively, when $\dot{\alpha}=\dot{\beta}=0$, η is fixed and smaller than M and N and the frictional destructuration has been completed ($\bar{S_f}=0$), hence $M_c^*=M_c$. Dafalias *et al.* [15] have presented the following closed-form relation for x_α:

$$\alpha_k=\frac{\eta}{x_\alpha}=\frac{B\varepsilon\eta_k^3+\eta_k^2+[2(1-\kappa/\lambda)-BM_c^2]\varepsilon\eta_k-M_c^2}{2\varepsilon(1-\kappa/\lambda)},\quad B=\frac{2(1+\nu)}{9(1-2\nu)}\frac{\kappa}{\lambda} \tag{69}$$

Different paths with $\eta_k=$constant correspond to different ε values, where $\varepsilon=\dot{\varepsilon}_v\dot{\varepsilon}_q$, i.e. the ratio of total strain rates. Of all possible such paths, the most frequently run is the K_0-loading path, for which $\varepsilon=3/2$ and $\eta_k=\eta_{k0}$. For the Bothkennar clay and for $\kappa=0.03$, $\lambda=0.255$, $M_c=1.4$ (at point B), $\nu=0.2$, and $\eta_{ko}=0.74$, Equation (69) yields $x_\alpha\simeq 3.14$. The parameter x_α allows the model to correctly capture exactly the measured value of K_0. The parameter x_β was set equal to 1 in order to the model to correctly capture the initial part of undrained stress path after an oedometric consolidation (recall Equation (69)). For a single surface version with associative flow rule, the x_β must be the same as x_α.

4.1.5. Initial values of state variables p_0^*, β, S_f, and (estimation of) α. In Figure 7 the symbols show the experimental results for the initial (*in-situ*) configuration of the yield surface for Sherbrook sample. A good estimation of the initial value of some model state variables can be obtained from this set of results. The solid line presents the estimated initial location of the yield surface in the model. It can be observed that, thanks to the proposed mathematical skewing that induces an apparent rotation of the elliptical yield surface supplemented by the large value of N_c^*, which characterizes the initially structured condition (frictional sensitivity $S_f\geqslant 1$), the rotated yield surface appears elongated as experimentally observed. This good model estimation of the initial yield surface is obtained using $p_0^*=53$ kPa, $\beta=0.7$, and $N_c^*=1.56$. Recalling from Figure 4(b) that $N=1.2$, the initial value of the frictional structuration factor can be estimated as $S_{f0}=N_c^*/N_c=1.3$. It is the opportunity to mention here the important advantage of having N or N^* different than M or M^*, because one can use appropriate values of the former in order to fit the experimentally determined yield points independently from the friction angle embodied in the values of the latter.

The choice of the initial value of α does not drastically affect the results, however, knowing the initial anisotropy in the plastic yield surface ($\beta=0.7$) one expects similar effect in the plastic potential (i.e. in α). For a rotationally stabilized state of the surfaces (e.g. already saturated under K_0 loading) it is know that $\alpha=\eta/x_\alpha=\beta/x_\alpha$. This relation can be used here for estimation of the initial value of α without introducing considerable error in the overall results, which yields $\alpha=\eta/x_\alpha=0.7/3.14\simeq 0.2$.

DOI: 10.1002/nag

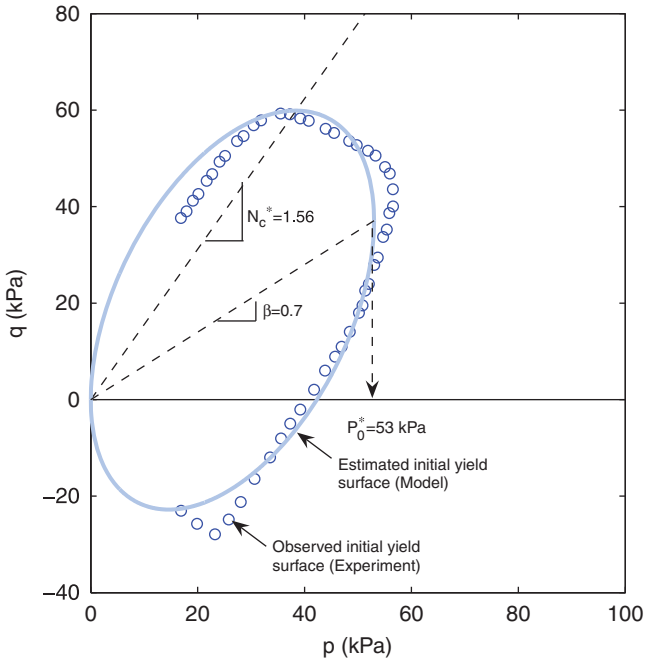

Figure 7. Calibration of initial values of internal variables p_0^*, β, and S_f based on *in-situ* state of soil.

4.1.6. Initial values of state variable S_i and estimation of parameters k_i and k_f. The best experiment for calibration of the initial value of S_i and the parameter k_i is an isotropic compression of an intact sample until complete loss of structure occurs. However, due to unavailability of such an experiment we use instead data of oedometric consolidation of Bothkennar clay. The observed behavior of Bothkennar clay in one-dimensional compression tests (8) is consistent with the general framework proposed in the literature for structured soils [26]: within the yield surface the stress–strain behavior is very stiff and mostly elastic with a low value of Poisson's ratio and, when yield occurs, compressibility increases rapidly, owing to loss of structure. Eventually a completely destructured state is obtained, which is characterized by a compressibility equal to that of the remoulded or reconstituted soil [34]. The initial stiff (elastic) part of response that falls within the yield surface can give a good estimate of the initial value of S_i, which approximately is the ratio of the axial (or confining) stress at the end of initial stiff regime and the corresponding stress on the LCC at the same void ratio. Figure 8(a) suggests that for the Bothkennar clay this ratio yields $S_{i0} \simeq 72/12 = 6$. The parameter k_i, which controls the rate of isotropic destructuration, is calibrated to $k_i = 0.9$ in Figure 8(b). Similarly (not shown here) the parameter k_f can be estimated given that the frictional sensitivity S_f should be exhausted during a one-dimensional compression path that brings the state from point A to point B, as previously discussed after Figure 4, and this assumption yields $k_f \simeq 1.3$. Of course larger values of k_f also provide the same result but then deteriorate the predictions in 8(b).

4.1.7. Parameters C. The calibration of constant C requires the execution of trial runs, having all other constants calibrated in advance. Observe that the constant C quantifies the rate of rotation

DOI: 10.1002/nag

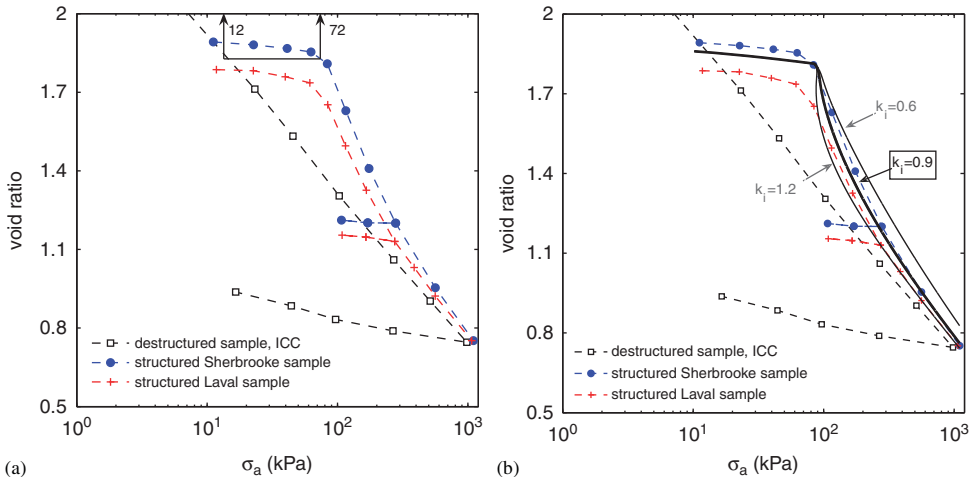

Figure 8. Calibration of initial values of (a) internal variable S_i and (b) constant k_i based on oedometer tests.

and distortion of the yield surface and the plastic potential surface in Equations (46) and (47). Hence, tests appropriate for its calibration are those that induce significant surface rotation, or in other words, tests for which the η_{in} is far from the final stress ratio η_f of the effective stress path, and possibly of opposite sign. Practically, a CKoUE test on normally consolidated clay is very suitable for the purpose at hand. Hence, Figure 9 presents the undrained extension tests on *in-situ* and K_0 consolidated as well as an undrained compression test on normally consolidated Bothkennar clay, along with a series of trial runs for $C=6$, 12, and 18. Observe that the higher the value of C, the larger the predicted undrained strength in the triaxial extension. For the Bothkennar clay in particular, $C=12$ appears most appropriate.

The foregoing calibration procedure for the Bothkennar clay provided the value of the model parameters and initial values of the state variables presented in Tables I and II. Nevertheless, the procedure itself is generic and should be considered appropriate for calibrating this model for any rate-independent sensitive clay with or without manifestation of destructuration during loading.

4.2. Simulations

This section presents the performance of the SANICLAY model with destructuration under various loading paths. The comparison of model simulations with the experimental results obtained on destructured sample as well as undisturbed (structured) samples of Bothkennar clay in one-dimensional compression are presented in Figure 10. Please note that the oedometric Intrinsic Compression Curve (ICC) in this figure is obtained by testing the reconstituted soil at initial slurry state (the procedure explained by Smith *et al.* [21]) and can be considered as the case in which the structuration of the sample has been already fully destroyed (i.e. $S_i=S_f=1$). Sherbrooke and Laval are two types of undisturbed specimens and the former appeared to suffer marginally less disturbance. The model response is fairly consistent with observations and a complete destructuration is correctly obtained only at very large stresses and strains.

Figure 11 compares model simulations with the experimental results of undrained triaxial compression and extension on Bothkennar samples at states A, B, C, and D (total of six

DOI: 10.1002/nag

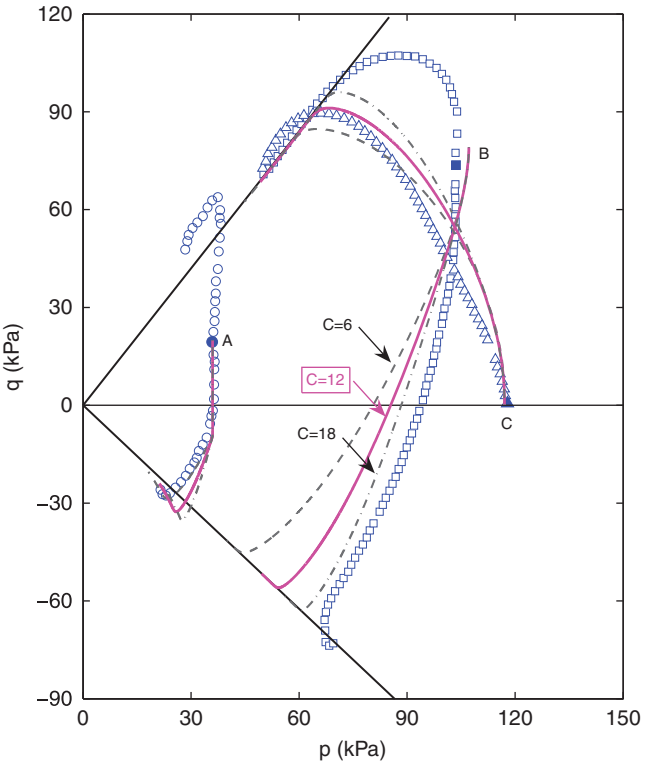

Figure 9. Calibration of constant C.

Table II. Initial conditions (model state variables) for undisturbed Bothkennar clay.

Variable	Description	Value
e	Initial void ratio	1.86
p_0^*	Defining the initial size of the yield surface	53
$\alpha(\beta)$	Initial orientation of the plastic potential (yield) surface	0.2 (0.7)
S_i	Initial volumetric structuration factor	6.0
S_f	Initial frictional structuration factor	1.3

stress paths). Out of this six stress pathes Smith *et al.* [21] have presented only the stress strain response of the samples that are sheared at the overconsolidated point A, for which model performance has been compared with the experimental results (see Figure 12). In fact for these later tests they have presented the stress–strain results from both Sherbrook and Laval samples.

In these two sets of figures, part (a) presents the simulations of the two-surface model version with the full set of parameters and initial states as presented in Tables I and II. Parts (b) and (c) present the model simulations for the two simplified versions of the model described in Section 3.4.1 for a two surface version with $M = N$ and in Section 3.4.2 for a single surface version. It can be observed that although these cases do not show the accuracy that was obtained in part (a)

DOI: 10.1002/nag

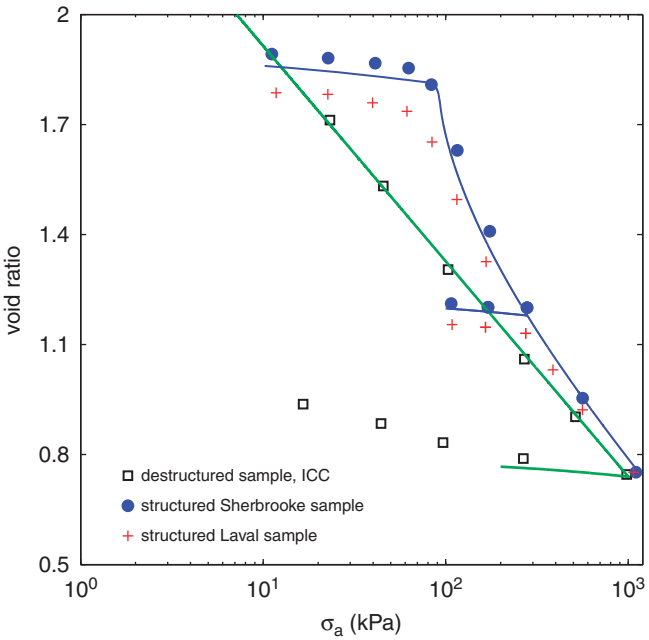

Figure 10. Comparison of model simulations (solid lines) with experimental data (symbols) for oedometric consolidation tests on destructured (reconstituted) and structured (undisturbed) samples of Bothkennar clay.

of these figures, still the results may be of acceptable level of accuracy from a practical point of view. Please note that these two model versions do not produce considerably different results for Figure 10 and that is why in this figure only simulations with the general form of the model (maximum freedom in choices of model parameters) are presented.

Finally, it is worth mentioning that in order to obtain a good match to the experimental results, in all of the present simulations the parameter A is chosen as 0.2 instead of the default value of 0.5. This parameter directly affects the rate of softening during destructuration in the stress–strain results of structured samples.

5. CONCLUSION AND DISCUSSION

The destructuration phenomenon for sensitive or structured clays can me modeled as a softening constitutive mechanism of the yield surface within an elastoplastic constitutive framework. As such it can be presented in a generic format appropriate for various forms of clay constitutive models, which was done in both the triaxial and multiaxial stress space at the beginning of this work. The novel element introduced in this development is the frictional destructuration addressing the decrease of the critical state friction angle via M, in addition to the classical isotropic destructuration addressing the reduction of the size of the yield surface as presented in numerous works preceding the current.

DOI: 10.1002/nag

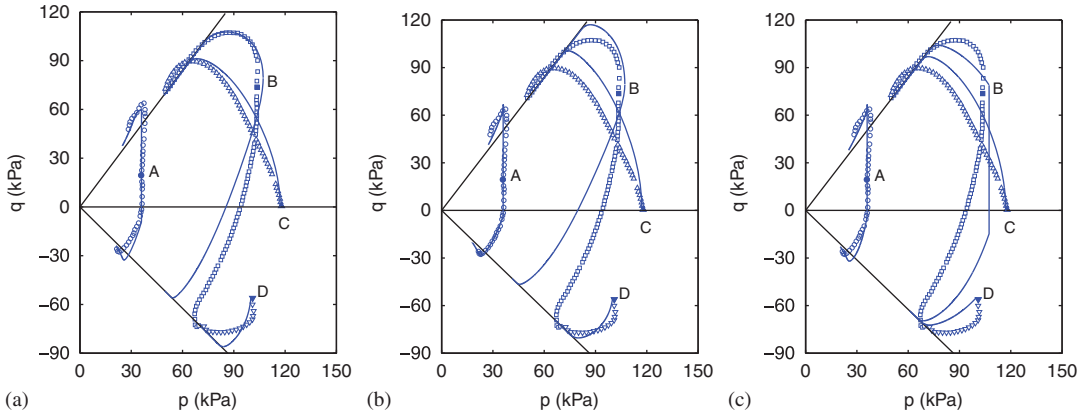

Figure 11. Comparison of model simulations (solid lines) with experimental data (symbols) for undrained stress paths of triaxial compression and extension tests on undisturbed Sherbrooke samples of Bothkennar clay following consolidation at points B (oedometrically consolidated), C (isotropically consolidated), D (passively consolidated) and A (*in-situ* state), using (a) two surface model with $N \neq M$; (b) two surface model with $N = M$; and (c) one surface model ($\circ, \square, \triangle, \triangledown$: Sherbrooke sample).

Subsequently the developed destructuration mechanism was incorporated into a slightly modified version of the SANICLAY model [15] and used to simulate the response of various loading paths of structures clays. Of interest is the comparison of the full model simulations with those of two simplified versions of it obtained by prescribing specific values to a number of parameters. Such a comparison shows that the full model yields better simulations of data but also the simplified versions provide an acceptable level of accuracy. In particular, the simplest version with the same yield and plastic potential surfaces and ensuing associative flow rule may be a good alternative to the full model for a very large scale computations.

A few more comments on deviatoric destruction are pertinent. For the structured material, isovolumetric plastic deformation (at a stress ratio $\eta = M$) does not necessarily imply that critical state has been reached. Indeed by definition critical state is yielding at constant stress and volume. Therefore, it can only be reached after complete destructuration (remoulding) of the soil. However, according to this model (or any plasticity model with associated or non-associated plastic flow), it is possible to reach the point of isovolumetric plastic deformations via a purely elastic stress path, and thus with no destructuration at all. Under subsequent isovolumetric plastic loading, destructuration could cause the stress ratio $\eta = M$ as well as the deviatoric stress q to change. Frictional destructuration has been introduced here to capture this possibility, because only isotropic destructuration would have caused the reduction of q but not of $\eta = M$. For the Bothkennar clay, the best fit frictional destructuration ratio of 1.3 implies that the stress ratio decreases under such loading. This suggests that structuration bonds in this clay are relatively more effective in resisting shear than istotropic compression. This is consistent with a more adhesive rather than purely repulsive nature of particle-to-particle interactions in the structured sample, which does not seem physically unreasonable. An attempt to simulate the response shown in Figures 10 and 11 neglecting all together the frictional destructuration and using only the isotropic resulted in a poorer fitting of the data.

DOI: 10.1002/nag

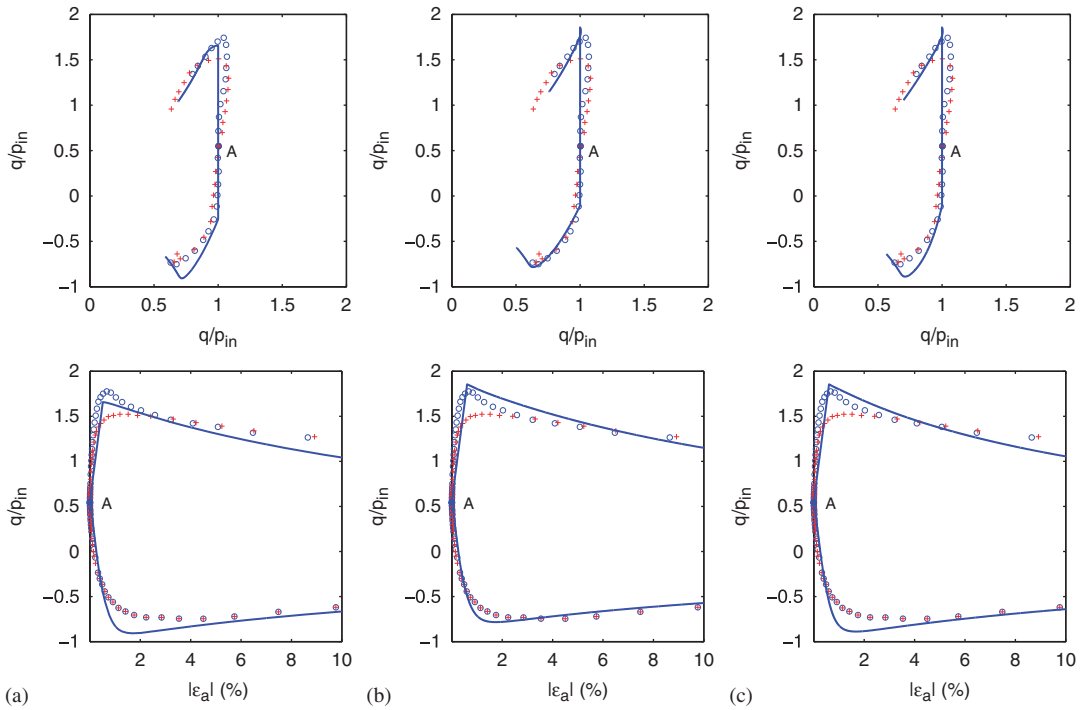

Figure 12. Comparison of model simulations (solid lines) with experimental data (symbols) for undrained stress path (detailed repetition of Figure 11) and the stress–strain curves of triaxial compression and extension tests on samples of Bothkennar clay following the *in-situ* state at point A, using (a) Two surface model with $N \neq M$; (b) two surface model with $N = M$; and (c) one surface model (○: Sherbrooke sample; +: Laval sample).

One issue that must be emphasized is that the calibration of a model for a structured clay cannot be simple. This is because one cannot obtain a truly intact sample from *in-situ* sampling since its sensitivity will alter the *in-situ* existing structure during the sampling process and the stressing up to the level of the *in-situ* stress. Thus, plausible assumptions and educated guesses are required for the level of destructuration before a laboratory experiment is performed for the purpose of calibrating the model constants. These aspects have been explained and exhibited during the calibration of the specific clays considered in this work.

ACKNOWLEDGEMENTS

Support for this study was provided by Shell Exploration and Production Company (USA) under the Planning and Technology Implementation management of John Pelletier, and the NSF grant No. CMS-0201231 of the program directed by Dr Richard Fragaszy. The authors acknowledge also the significant and thoughtful input of the anonymous reviewers.

DOI: 10.1002/nag

REFERENCES

1. Burland JB. The yielding and dilation of clay. *Géotechnique* 1965; **15**(2):211–214.
2. Zdravković L, Potts DM, Hight DW. The effect of strength anisotropy on the behaviour of embankments on soft ground. *Géotechnique* 2002; **52**(6):447–457.
3. Leroueil S, Tavenas F, Brucy F, La Rochelle P, Roy M. Behaviour of destructured natural clays. *Journal of Geotechnical Engineering Division* (ASCE) 1979; **105**(6):759–778.
4. Sekiguchi H, Ohta K. Induced anisotropy and time dependence in clays. *Constitutive Equations for Soils*, *Proceedings of 9th ICSMFE* (*Specialty Session 9*), Tokyo, 1977; 229–238. JSSMFE.
5. Hashiguchi K. An expression of anisotropy in plastic constitutive equations of soils. *Constitutive Equations for Soils*, *Proceedings of 9th ICSMFE* (*Specialty Session 9*), Tokyo, 1977; 302–305. JSSMFE.
6. Dafalias YF. An anisotropic critical state soil plasticity model. *Mechanics Research Communications* 1986; **13**(6):341–347.
7. Dafalias YF. An anisotropic critical state clay plasticity model. In *Constitutive Laws for Engineering Materials*: *Theory and Applications*, *Proceedings of 2nd IC*, New York, Desai CS *et al.* (eds). Elsevier: Amsterdam, 1987; 513–521.
8. Korhonen KH, Lojander M. Yieldign of perno clay. In *Constitutive Laws for Engineering Materials*: *Theory and Applications*, *Proceedings of 2nd IC*, New York, Desai CS *et al.* (eds), vol. II. Elsevier: Amsterdam, 1987; 1249–1255.
9. Thevanayagam S, Chameau JL. Modelling anisotropy of clays at critical state. *Journal of Engineering Mechanics* (ASCE) 1992; **118**(4):786–806.
10. Newson TA, Davies MCR. A rotational hardening constitutive model for anisotropically consolidated clay. *Soils and Foundations* 1996; **36**(3):13–20.
11. Wheeler SJ, Karstunen M, Näätänen A. Anisotropic hardening model for normally consolidated soft clays. In *Numerical Models in Geomechanics*, *Proceedings of NUMOG VII*, Pande GN, Pietruszczak S, Schweiger HF (eds), vol. II. Balkema: Rotterdam, 1999; 33–40.
12. Wheeler SJ, Näätänen A, Karstunen M, Lojander M. An anisotropic elastoplastic model for soft clays. *Canadian Geotechnical Journal* 2003; **40**:403–418.
13. Dafalias YF, Manzari MT, Akaishi M. A simple anisotropic clay plasticity model. *Mechanics Research Communications* 2002; **29**(6):241–245.
14. Dafalias YF, Papadimitriou AG, Manzari MT. Simple anisotropic plasticity model for soft clays. In *Proceedings of the International Workshop on Geotechnics of Soft Soils—Theory and Practice*, Vermeer D, Schweiger D, Karstunen D, Cudny D (eds). Noordwijkerhout, The Netherlands, 2003.
15. Dafalias YF, Manzari MT, Papadimitriou AG. SANICLAY: simple anisotropic clay plasticity model. *International Journal for Numerical and Analytical Methods in Geomechanics* 2006; **30**(12):1231–1257.
16. Terzaghi K. Ends and means in soil mechanics. *Engineering Journal* (*Canada*) 1944; **27**:608.
17. Skempton A, Northey R. The sensitivity of clays. *Géotechnique* 1952; **3**:30–52.
18. Burland JB. On the compressibility and shear strength of natural clays. *Géotechnique* 1990; **40**(3):329–378.
19. Wheeler SJ, Cudny M, Neher HP, Wiltafsky C. Some developments in constitutive modelling of soft clays. In *Proceedings of the International Workshop on Geotechnics of Soft Soils—Theory and Practice*, Vermeer D, Schweiger D, Karstunen D, Cudny D (eds). Noordwijkerhout, The Netherlands, 2003.
20. Mitchell RJ. On the yielding and mechanical strength of leda clay. *Canadian Geotechnical Journal* 1970; **7**(3):297–312.
21. Smith PR, Jardine RJ, Hight DW. Yielding of bothkennar clay. *Géotechnique* 1992; **42**(2):257–274.
22. Callisto L, Calabresi G. Mechanical behaviour of a natural soft clay. *Géotechnique* 1998; **48**(4):495–513.
23. Burland JB, Rampello S, Georgiannou VN, Calabresi G. A laboratory study of the strength of four stiff clays. *Géotechnique* 1996; **46**(3):491–514.
24. Rampello S, Georgiannou VN, Viggiani G. Strength and dilatancy of natural and reconstituted vallericca clay. In *Geotechnical Engineering of Hard Soils Soft Rocks*: *Proceedings of an International Symposium under the Auspices of the ISSMFE*, Athens, 20–23 September, Anagnostopoulos A, Schlosser F, Kalteziotis N, Frank R (eds), vol. 1. A.A. Balkema: Rotterdam, The Netherlands, 1993; 761–768.
25. Cotecchia F, Chandler J. A general framework for the mechanical behaviour of clays. *Géotechnique* 2000; **50**(4):431–447.
26. Leroueil S, Vaughan PR. The general and congruent effects of structure in natural soils and weak rocks. *Géotechnique* 1990; **40**(3):467–488.

DOI: 10.1002/nag

27. Bjerrum L. Kvikkleireskred. et studium av årsaksforhold og forbygningsmuligheter (quick clay slides: a study of causes and controls), *Technical Report NGI pub. 89*, Norwegian Geotechnical Institute, Norway, 1971; 4.
28. Oka F, Leroueil S, Tavenas F. A constitutive model for natural soft clays with strain hardening. *Soils and Foundations* 1989; **29**(3):54–66.
29. Gens A, Nova R. Conceptual bases for a constitutive model for bounded soils and weak rocks. In *Geomechanical Engineering of Hard Soils and Soft Rocks*, Anagnostopoulos A, Schlosser F, Kaltesiotis N, Frank R (eds), vol. 1. A.A. Balkema: Rotterdam, 1993; 485–494.
30. Nova R. Mathematical modelling of natural and engineered geomaterials. *European Journal of Mechanics A*: *Solids* 1992; **11**:135–154.
31. Lagioia R, Nova R. An experimental and theoretical study of the behaviour of a calcarenite in triaxial compression. *Géotechnique* 1995; **45**(4):633–648.
32. Rouainia M, Muir Wood D. A kinematic hardening constitutive model for natural clays with loss of structure. *Géotechnique* 2000; **50**(2):153–164.
33. Kavvadas M, Amorosi A. A constitutive model for structured soils. *Géotechnique* 2000; **50**(3):263–273.
34. Gajo A, Wood DM. A new approach to anisotropic, bounding surface plasticity: general formulation and simulations of natural and reconstituted clay behaviour. *International Journal for Numerical and Analytical Methods in Geomechanics* 2001; **25**(3):207–241.
35. Amorosi A, Kavvadas M. A critical review of the state boundary surface concept in light of advanced constitutive modelling. In *Numerical Models in Geomechanics* (*NUMOG*), *Proceedings of NUMOG VIII*, Pande GN, Pietruszczak S, Schweiger HF (eds). Balkema: Rotterdam, 2002; 85–90.
36. Callisto L, Gajo A, Wood DM. Simulation of triaxial and true triaxial tests on natural and reconstituted pisa clay. *Géotechnique* 2002; **52**(9):649–666.
37. Liu MD, Carter JP. A structured cam clay model. *Canadian Geotechnical Journal* 2002; **39**(6):1313–1332.
38. Callisto L, Rampello S. An interpretation of structural degradation for three natural clays. *Géotechnique* 2004; **41**:392–407.
39. Baudet BA, Stallebrass SE. A constitutive model for structured clays. *Géotechnique* 2004; **54**(4):269–278.
40. Baudet BA, Stallebrass SE. Modelling the destructuration of soft natural clays. *Proceedings of the 10th International Conference on Computer Methods and Advances in Geomechanics*, Tucson, vol. 1, 2001; 297–301.
41. Argyris JH, Faust G, Szimmat J, Warnke EP, Willam KJ. Recent developments in the finite element analysis of prestressed concrete reactor vessels. *Nuclear Engineering and Design* 1974; **282**(1):42–75.
42. Gens A. Stress–strain and strength of a low plasticity clay. *Ph.D. Thesis*, Imperial College, London University, 1982; 856.
43. Allman MA, Atkinson JH. Mechanical properties of reconstituted bothkennar soil. *Géotechnique* 1992; **42**(2): 289–301.

DOI: 10.1002/nag